

Families of solitons in Bragg supergratings

Boris A. Malomed

Department of Physical Electronics, School of Electrical Engineering, Faculty of Engineering, Tel Aviv University, Tel Aviv 69978, Israel

Thomas Wagenknecht

Department of Applied Mathematics, University of Leeds, Leeds LS2 9JT, UK

Kazuyuki Yagasaki*

Mathematics Division, Department of Information Engineering, Niigata University, Niigata 950-2181, Japan

Abstract

We study fundamental optical gap solitons in the model of a fiber Bragg grating (BG), which is subjected to a periodic modulation of the local reflectivity, giving rise to a supergrating. In addition, the local refractive index is also periodically modulated with the same period. It is known that the supergrating opens an infinite system of new bandgaps in the BG's spectrum. We use a combination of analytical and computational methods to show that each emerging bandgap is filled with gap solitons (GSs), including asymmetric ones and bound states of the GSs. In particular, bifurcations of the GSs created by the supergrating are studied in terms of a geometric analysis.

Keywords: Gap soliton, supergrating, homoclinic orbit, Melnikov method, averaging method

1. Introduction

Bragg gratings (BGs) are light-controlling structures produced by a periodic variation of the refractive index along an optical fiber or waveguide. Devices based on fiber gratings, such as dispersion compensators, sensors, elements of laser cavities, etc., are widely used in optical systems [21]. Gap solitons (GSs) in fiber gratings, alias BG solitons [10], are supported through the balance between the BG-induced dispersion, which incorporates the bandgap in the system's linear spectrum, and the Kerr nonlinearity of the fiber or waveguide. Analytical solutions for BG solitons in the standard fiber-grating model are well known [1, 7]. Slightly more than half of the analytical found family is stable, as first demonstrated, within the framework

*Corresponding author

Email addresses: malomed@post.tau.ac.il (Boris A. Malomed), thomas@maths.leeds.ac.uk (Thomas Wagenknecht), yagasaki@ie.niigata-u.ac.jp (Kazuyuki Yagasaki)

of the variational approximation, in Ref. [26], and then in a consistent numerical form in Ref. [3]. Later, an accurate numerical technique for simulations of GSs was elaborated in Ref. [9], and a rigorous analysis of their stability was developed in Ref. [8]

Following the theoretical prediction, BG solitons were created in the experiment, using a relatively short BG written in the cladding of an optical fiber [15] and a virtual optically-induced grating [39]. In particular, an essential physical achievement was the creation of slow BG solitons moving at the velocity much lower than the velocity of light c in vacuum (namely, $0.16c$ [27]).

GSs are one of fundamental species of solitons in optics, as well as in other nonlinear media. In particular, the GS concept was extended to Bose-Einstein condensates (BECs), where such solitons were predicted in a condensate loaded into a periodic potential (optical lattice) [2, 4, 31], and then created in the experiment [16].

An issue of great significance to the fundamental studies and applications is the development of methods for control of BG solitons. One of them is *apodization* [14, 25, 27, 36], i.e., the use of a grating with the Bragg reflectivity gradually varying along the fiber (or waveguide). In particular, a possibility was predicted to slow down the soliton and eventually bring it to a halt in a properly apodized BG [25]. Experimentally, it has been shown that the apodization helps to couple solitons into fiber gratings [14], and may also split them [36]. The retardation of the BG solitons to the above-mentioned low velocity, $0.16c$, was also performed with the help of the apodization [27].

Technologies which make it possible to fabricate regular fiber gratings with periodic apodization, i.e., an effective *superlattice* built on top of the BG, are well established [35]. Analysis of the light propagation in the so developed *supergratings* was performed in [5]. It was shown that the supergrating gives rise to extra gaps in the system's spectrum ("Rowland ghost gaps"). Solitons in the gaps were looked for in an approximation based on "supercoupled-mode equations", which, essentially, assume that a soliton amounts to a slowly varying envelope of the supergrating's Bloch function(s). As is known, such an approximation (the averaging method) generally applies to the description of GSs near bandgap edges [4]. A related problem was considered in [24, 34], *viz.*, GSs in the BEC loaded into a double-periodic optical lattice. The period doubling opens an additional narrow "mini-gap", where stable GSs exist.

The objective of our work is to investigate the existence of GSs in harmonic superlattices created on top of the usual BG in fibers or waveguides with the intrinsic Kerr nonlinearity, extending the analysis initiated in [49]. Our model has periodic potentials in one spatial dimension. Analytical approaches for GSs in two or more spatial dimensions were also developed recently in [12, 13, 19, 32].

The paper is organized as follows. We first give our mathematical model of the supergrating and analyze the bandgap structure in the model, using its dispersion relation, in Section 2. This constitutes a non-trivial extension of the classical spectral theory for the Mathieu equation [37], and predicts parameter values at which GSs may be expected to exist in the model. The sequence of new bandgaps not present in the

unmodulated BG is produced.

In Sections 3 and 4 we establish the existence of GSs in the newly opened bandgaps, using a combination of analytical and numerical techniques. We find various families of GSs in the supergrating, including those which do not exist in the ordinary GS model (in particular, stable asymmetric solitons, and multi-soliton bound states). Using the Melnikov method, we first prove that GSs in the original BG model have counterparts in the extended model. A similar treatment was used for a perturbed Hamiltonian partial differential equations in [20]. Then, the method of averaging is used to demonstrate the emergence of GSs in the new bandgaps. The most important result is that in each new bandgap, there is a single family of fundamental symmetric GSs which *entirely* fills the gap. Such GSs near band edges in nonlinear Schrödinger equations with periodic potentials were also studied by different approaches in [18, 33]. In Section 5 we discuss bifurcations of GSs from a geometric point of view and illustrate this general approach in numerical computations for our problem.

The majority of the newly established GSs are *stable* solutions of the model equations. In particular, the family of fundamental GSs in the new bandgaps is stable even for negative frequencies, when the ordinary GSs are unstable [3, 26]. We do not study the stability of GSs in this paper in detail, referring to [49] for the verification of the stability by means of direct simulations.

2. Preliminaries

2.1. The supergrating equations

The standard model of the Bragg grating (BG) in an optical fiber is based on the equations [7]

$$\begin{aligned} iu_t + iu_x + v + (|v|^2 + \frac{1}{2}|u|^2) u &= 0, \\ iv_t - iv_x + u + (|u|^2 + \frac{1}{2}|v|^2) v &= 0, \end{aligned} \tag{2.1}$$

where u and v are amplitudes of the right- and left-propagating waves in the fiber. In these equations, x is the coordinate along the fiber, and t is time. A family of exact soliton solutions of (2.1) have been found in [1, 7].

Here we will consider a situation where the BG is subjected to periodic modulation in x , with a period $2\pi/k$, which gives rise to a *supergrating*. The general form of the extended model reads

$$\begin{aligned} iu_t + iu_x + [1 - \varepsilon \cos(kx)] v + \mu \cos(kx + \delta) u + (|v|^2 + \frac{1}{2}|u|^2) u &= 0, \\ iv_t - iv_x + [1 - \varepsilon \cos(kx)] u + \mu \cos(kx + \delta) v + (|u|^2 + \frac{1}{2}|v|^2) v &= 0. \end{aligned} \tag{2.2}$$

The real parameter $\varepsilon > 0$ accounts for the periodic modulation of the BG strength. In real fiber gratings, it may be typically 1 cm [5, 35], while the total length of the grating may be up to 1 m. The modulation is implemented through the change imposed on the local variation of the refractive index in the fiber's cladding

and may also affect the local index felt by each wave. This is accounted for by the perturbation parameter $\mu \geq 0$ and a phase shift δ . In practice, the harmonic superlattice corresponding to Eqs. (2.2) may be implemented if the optical interference pattern, which is used to burn the grating into the fiber, is created with spatial beatings. We consider stationary GSs, which are found via the ansatz

$$u(x, t) = \exp(-i\omega t)U(x), \quad v(x, t) = \exp(-i\omega t)V(x).$$

Substituting this into Eqs. (2.2), we obtain

$$\begin{aligned} \omega U + iU' + [1 - \varepsilon \cos(kx)]V + \mu \cos(kx + \delta)U + (|V|^2 + \frac{1}{2}|U|^2)U &= 0, \\ \omega V - iV' + [1 - \varepsilon \cos(kx)]U + \mu \cos(kx + \delta)V + (|U|^2 + \frac{1}{2}|V|^2)V &= 0, \end{aligned} \tag{2.3}$$

where the prime stands for d/dx .

2.2. Linear analysis

We first analyze the bandgap structure of (2.2) by looking for solutions of the linearized system in the form of

$$u(x, t) = \exp(iqx - i\omega t)U(x), \quad v(x, t) = \exp(iqx - i\omega t)V(x),$$

with q being the propagation constant. Thus, we have to find periodic solutions of the linearization of (2.3)

$$\begin{aligned} (\omega - q)U + iU' + [1 - \varepsilon \cos(kx)]V + \mu \cos(kx + \delta)U &= 0, \\ (\omega + q)V - iV' + [1 - \varepsilon \cos(kx)]U + \mu \cos(kx + \delta)V &= 0. \end{aligned} \tag{2.4}$$

Note that in the unperturbed problem, with $\varepsilon, \mu = 0$, the dispersion relation is given by $\omega^2 = q^2 + 1$, so that we find the well-known gap in the spectrum $-1 < \omega < 1$.

Let us consider the case of $\mu = 0$. For $\varepsilon > 0$ non-trivial solutions of (2.4) emerge due to parametric resonance, similar to the situation in the classical Mathieu equation [37]. Consequently, we expect new gaps to open up at points $\omega_{\pm m} = \pm\sqrt{1 + (mk)^2/4}$, $m = \pm 1, \pm 2, \dots$. We will denote the corresponding gaps by $\mathbf{1}^\pm, \mathbf{2}^\pm, \dots$, while the central gap will be denoted by $\mathbf{0}$. In the central gap $\mathbf{0}$, GSs for $\varepsilon, \mu \neq 0$ are found as perturbations of the soliton for $\varepsilon, \mu = 0$, established in [1]. We will use Melnikov's method [17] to prove the existence of gap solitons in Section 3. For the non-central gaps, however, we will apply the averaging method to investigate the emergence of (small) GSs for $\varepsilon, \mu \neq 0$ in Section 4.

Straightforward perturbation theory for parametrically excited systems yields approximation to the gaps for small $\varepsilon > 0$. For example, an approximation to the gap with ω close to $\omega_{\pm 1}$, i.e. close to the unperturbed first gap at $\varepsilon = 0$, can be obtained by looking for solutions of (2.4) to lowest order approximation

$$\begin{aligned} U(x) &= A + \alpha_1 \cos(kx) + \alpha_2 \sin(kx), \\ V(x) &= A + \beta_1 \cos(kx) + \beta_2 \sin(kx). \end{aligned}$$

Using this ansatz we derive at the solvability condition at order $O(\varepsilon^2)$,

$$\begin{aligned} & (\omega^2 - q^2 - 1) [(\omega^2 - q^2 - 1 - k^2)^2 - 4k^2q^2] \\ & = \varepsilon^2 [(\omega^2 - q^2)^2 - k^2(\omega^2 + q^2 + 1) - 1]. \end{aligned} \quad (2.5)$$

Observe that $\omega^2 \approx q^2 + 1$, since we are interested in the gap close to the unperturbed one with $\varepsilon = 0$. Moreover, note that at the boundaries of the gaps periodic solutions with wavenumber k or $k/2$ exist [37]. Hence, being interested in solutions with $q \approx k/2$ we introduce

$$P := \omega^2 - q^2 - 1, \quad Q := k^2 - 4q^2,$$

and expand (2.5) for small P, Q to obtain

$$2k^2P^2 + ((k^2 - 2)\varepsilon^2 - k^2Q)P + 2k^2(q^2 + 1)\varepsilon^2 = 0.$$

A new gap appears if this quadratic equation for P has no real solutions. Thus we obtain as the condition for the gap, that

$$\left| Q - \frac{k^2 - 2}{k^2} \varepsilon^2 \right| < 2\varepsilon \sqrt{k^2 + 4}.$$

In terms of the original parameter ω we find that the gaps open up at $\omega_{\pm 1} = \sqrt{1 + k^2/4}$ and their widths are

$$\Delta\omega = \frac{q\Delta q}{\omega} = \frac{k}{2}\varepsilon.$$

Similar expressions can be obtained for the higher-order gaps \mathbf{m}^{\pm} for $m \geq 2$ showing that the gap width of the band corresponding to m scales with $\varepsilon^{|m|}$. We can treat the case of $\mu \neq 0$ similarly.

These perturbative results can be extended numerically by detecting parameter values, for which Eqs. (2.4) possesses periodic solutions with wavenumber k or $k/2$. It is well known that these parameters form the boundary of the gaps in the spectrum (compare with above).

Following [38] we have computed these parameter values as solutions of the corresponding eigenvalue problem in Matlab. The results for several combinations of parameter values k and μ are shown in Fig. 1. In this figure the shaded and white areas stand for bands and gaps, respectively. It is found that varying k merely changes the width of bands and gaps with respect to ω , whereas changing μ leads to more complex effects. In particular, for $\mu \neq 0$ gaps opening at $\varepsilon, \mu = 0$ can vanish again when ε or μ are increased.

3. Existence of gap solitons in the central gap

In this and next sections we investigate the existence of GSs in Eq. (2.2), using both analytical and numerical techniques. These solitons are described by homoclinic solutions to the origin $(U, V) = (0, 0)$ in Eqs. (2.3).

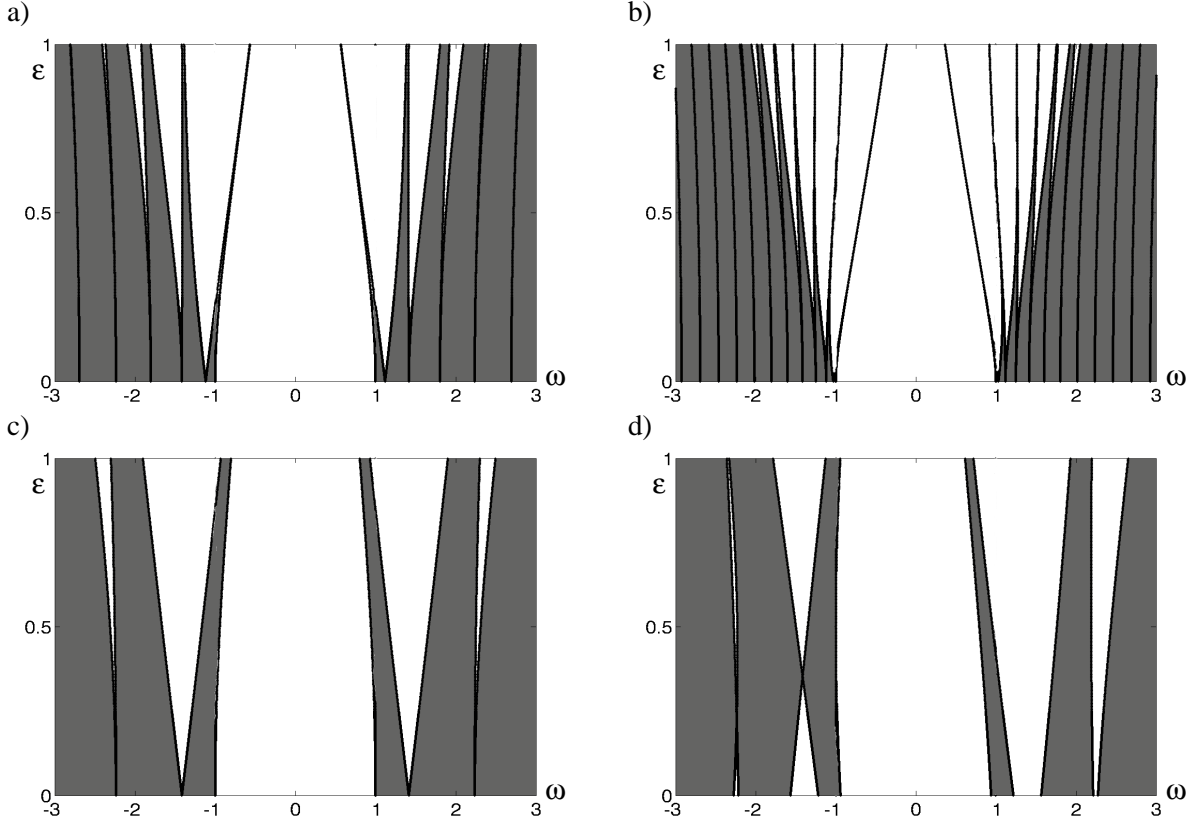


Figure 1: The linear spectrum of Eq. (2.4) in the (ω, ε) plane. Shaded and white areas are, respectively, bands and gaps. The diagrams show the spectrum for a) $k = 1, \mu = 0$, b) $k = 0.5, \mu = 0$, c) $k = 2, \mu = 0$, and d) $k = 2, \mu = 0.5, \delta = 0$.

Before we present the computations let us take a closer look at properties of Eqs. (2.3). It will be important that these equations allow for a symmetry reduction by setting $V = -U^*$, where '*' denotes complex conjugation. In the following, we will thus only consider the reduced equation

$$iU' + \omega U - (1 - \varepsilon \cos kx)U^* + \mu \cos(kx + \delta)U + \frac{3}{2}|U|^2U = 0. \quad (3.1)$$

Let $U = a + ib$, where $a, b \in \mathbb{R}$. Eq. (3.1) is rewritten as

$$\begin{aligned} a' &= -[\omega + 1 - \varepsilon \cos kx + \mu \cos(kx + \delta)]b - \frac{3}{2}(a^2 + b^2)b, \\ b' &= [\omega - 1 + \varepsilon \cos kx + \mu \cos(kx + \delta)]a + \frac{3}{2}(a^2 + b^2)a. \end{aligned} \quad (3.2)$$

We will consider (3.2) as a dynamical system in the three-dimensional phase space $\mathbb{R}^2 \times \mathbb{S}^1$, with \mathbb{S}^1 as the circle of length $2\pi/k$.

Note that if $\mu \sin \delta = 0$, then Eqs. (3.2) are *reversible*, that is, invariant under compositions of time

reversal and the (linear) involutions,

$$\begin{aligned} R_1 : (a, b, x) &\mapsto (a, -b, -x), & R'_1 : \left(a, b, x - \frac{\pi}{k}\right) &\mapsto \left(a, -b, \frac{\pi}{k} - x\right), \\ R_2 : (a, b, x) &\mapsto (-a, b, -x), & R'_2 : \left(a, b, x - \frac{\pi}{k}\right) &\mapsto \left(-a, b, \frac{\pi}{k} - x\right). \end{aligned}$$

We refer to [23] for a general review of reversible systems. Of particular importance for us will be *symmetric* homoclinic orbits, which are mapped to itself under the action of $R_{1,2}$ or $R'_{1,2}$. It is well known that an orbit is symmetric if and only if it intersects the invariant plane of the involution.

Now we assume that $0 \leq \varepsilon, \mu \ll 1$ and $-1 < \omega < 1$, and set $\omega = \cos \theta$ for some $\theta \in (0, \pi)$. The cases of $|\omega| > 1$ and $|\omega| \approx 1$ will be treated in Section 4 and Appendix B, respectively.

For $\varepsilon, \mu = 0$ Eqs. (3.2) become a planar Hamiltonian system,

$$\begin{aligned} a' &= -(\omega + 1)b - \frac{3}{2}(a^2 + b^2)b, \\ b' &= (\omega - 1)a + \frac{3}{2}(a^2 + b^2)a, \end{aligned} \tag{3.3}$$

with a Hamiltonian

$$H(a, b) = \frac{1}{2}[(\omega - 1)a^2 + (\omega + 1)b^2] + \frac{3}{8}(a^2 + b^2)^2,$$

where a and b represent the canonical momentum and coordinates, respectively. The equilibrium at the origin is a hyperbolic saddle in (3.3) and has a pair of homoclinic orbits

$$\begin{aligned} (a_{\pm}(x), b_{\pm}(x)) &= \left(\pm 2\sqrt{\frac{2}{3}} \sin \theta \cos\left(\frac{\theta}{2}\right) \frac{\cosh(x \sin \theta)}{\cosh(2x \sin \theta) + \cos \theta}, \right. \\ &\quad \left. \pm 2\sqrt{\frac{2}{3}} \sin \theta \sin\left(\frac{\theta}{2}\right) \frac{\sinh(x \sin \theta)}{\cosh(2x \sin \theta) + \cos \theta} \right), \end{aligned} \tag{3.4}$$

which are symmetric under the involution R_1 . When ε and/or μ are nonzero but sufficiently small, the origin is still a hyperbolic saddle in (3.2) and has two-dimensional stable and unstable manifolds which may intersect transversely. Such intersection yields transverse homoclinic orbits to the saddle at the origin, which persist under variation of the parameters [41]. Along certain curves in the parameter space, however, the intersection of the manifolds may become tangential, resulting in bifurcations of the homoclinic orbits. See Section 5 for details.

Here we aim to prove the existence of such transverse homoclinic orbits in Eqs. (3.2) by means of the Melnikov method [17]. From formula (4.5.6) in [17], we derive the Melnikov functions $M_{\pm}(x_0)$ for

$(a_{\pm}(x), b_{\pm}(x))$ as

$$\begin{aligned}
M_{\pm}(x_0) &= \varepsilon \int_{-\infty}^{\infty} [2\omega + 3(a_{\pm}^2(x) + b_{\pm}^2(x))] a_{\pm}(x) b_{\pm}(x) \cos k(x + x_0) dx \\
&\quad + 2\mu \int_{-\infty}^{\infty} a_{\pm}(x) b_{\pm}(x) \cos[k(x + x_0) + \delta] dx \\
&= -\varepsilon \left(\int_{-\infty}^{\infty} [2\omega + 3(a_{\pm}^2(x) + b_{\pm}^2(x))] a_{\pm}(x) b_{\pm}(x) \sin kx dx \right) \sin kx_0 \\
&\quad - 2\mu \left(\int_{-\infty}^{\infty} a_{\pm}(x) b_{\pm}(x) \sin kx dx \right) \sin(kx_0 + \delta), \tag{3.5}
\end{aligned}$$

where we used the fact that $a_{\pm}(x)$ and $b_{\pm}(x)$ are even and odd functions of x , respectively. Substituting (3.4) into (3.5) and using the method of residues, we compute

$$\begin{aligned}
&\int_{-\infty}^{\infty} a_{\pm}(x) b_{\pm}(x) \sin kx dx \\
&= \frac{2}{3} \sin^3 \theta \int_{-\infty}^{\infty} \frac{\sinh(2x \sin \theta)}{[\cosh(2x \sin \theta) + \cos \theta]^2} \sin kx dx \\
&= \frac{\pi k}{3} \operatorname{cosech} \left(\frac{k\pi}{2 \sin \theta} \right) \sinh \left(\frac{k\theta}{2 \sin \theta} \right) \tag{3.6}
\end{aligned}$$

and

$$\begin{aligned}
&\int_{-\infty}^{\infty} [a_{\pm}^2(x) + b_{\pm}^2(x)] a_{\pm}(x) b_{\pm}(x) \sin kx dx \\
&= \frac{8}{9} \sin^5 \theta \int_{-\infty}^{\infty} \frac{\sinh(2x \sin \theta)}{[\cosh(2x \sin \theta) + \cos \theta]^3} \sin kx dx \\
&= \frac{\pi k}{9} \operatorname{cosech} \left(\frac{k\pi}{2 \sin \theta} \right) \left[-2 \sinh \left(\frac{k\theta}{2 \sin \theta} \right) \cos \theta + k \cosh \left(\frac{k\theta}{2 \sin \theta} \right) \right]. \tag{3.7}
\end{aligned}$$

See Appendix A for derivations of (3.6) and (3.7). Hence, the Melnikov functions become

$$\begin{aligned}
M_{\pm}(x_0) &= -\frac{\pi k^2}{3} \varepsilon \operatorname{cosech} \left(\frac{k\pi}{2 \sin \theta} \right) \cosh \left(\frac{k\theta}{2 \sin \theta} \right) \sin kx_0 \\
&\quad - \frac{2\pi k}{3} \mu \operatorname{cosech} \left(\frac{k\pi}{2 \sin \theta} \right) \sinh \left(\frac{k\theta}{2 \sin \theta} \right) \sin(kx_0 + \delta),
\end{aligned}$$

where we used the relation $\omega = \cos \theta$.

Let us assume that

$$\delta \neq \pi \quad \text{or} \quad \varepsilon \neq \frac{2\mu}{k} \tanh \left(\frac{k\theta}{2 \sin \theta} \right). \tag{3.8}$$

Then we easily see that $M_{\pm}(x_0)$ has simple zeros at

$$x_0 = \bar{x}_0, \quad \bar{x}_0 + \frac{\pi}{k} \pmod{\frac{2\pi}{k}}, \tag{3.9}$$

where

$$\bar{x}_0 = -\frac{1}{k} \arctan \left(\frac{2\mu \sin \delta}{2\mu \cos \delta + k\varepsilon \coth(k\theta/2 \sin \theta)} \right).$$

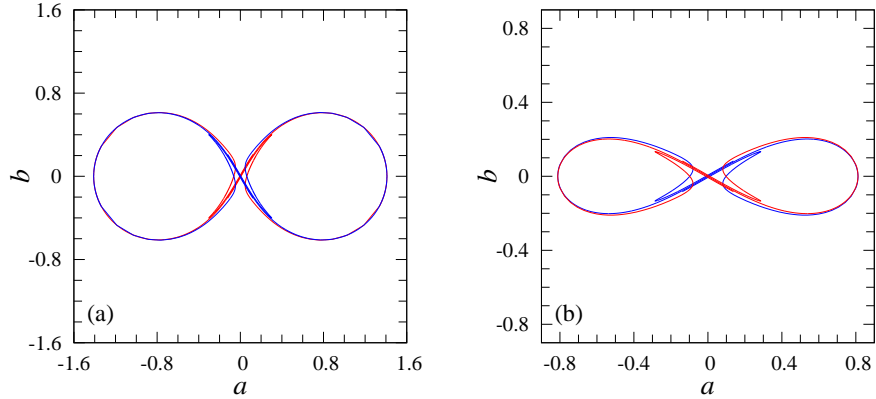


Figure 2: Stable manifold (red) and unstable manifold (blue) of the origin in the Poincaré section $x = 0 \pmod{2\pi}$ for $\varepsilon = 0.01$, $\mu = 0$ and $k = 1$: (a) $\omega = -0.5$; (b) $\omega = 0.5$.

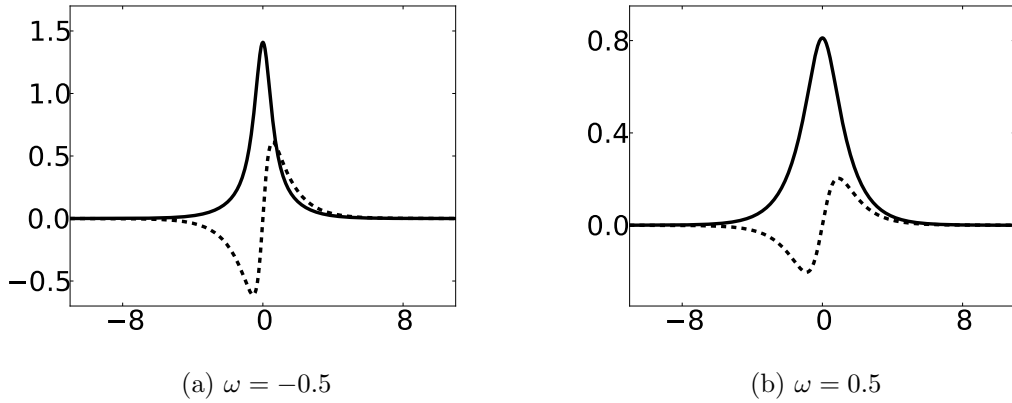


Figure 3: Symmetric GSs with $V = -U^*$ of (2.2) in the central gap with $k = 1$, $\varepsilon = 0.01$ and $\mu = 0$. The solid curve shows the real part and the dashed curve the imaginary part of the solution.

This implies that there exist transverse homoclinic orbits near $(a, b) = (a_{\pm}(x - \bar{x}_0), b_{\pm}(x - \bar{x}_0))$ and $(a_{\pm}(x - \bar{x}_0 - \pi/k), b_{\pm}(x - \bar{x}_0 - \pi/k))$. In particular, when $\mu \sin \delta = 0$, we have $\bar{x}_0 = 0$ so that the first and second orbit are symmetric under R_1 and R_2 , respectively. Thus, we can prove that there exist GSs with $V = -U^*$ in (2.2).

To illustrate the above analysis we now introduce the Poincaré section $\{x = 0 \pmod{2\pi}\}$ in phase space, and consider the return map induced by the flow of (3.2). We have computed the stable and unstable manifolds of the origin using the continuation tool AUTO [11] with assistance of the HomMap driver [43, 44]. In particular, to compute the stable and unstable manifolds, small segments ($\sim 10^{-5}$) in the stable and unstable subspaces of the origin were taken and solutions of (3.2) with initial conditions on the segments were numerically integrated. The same approach was also used for computation of the one-dimensional

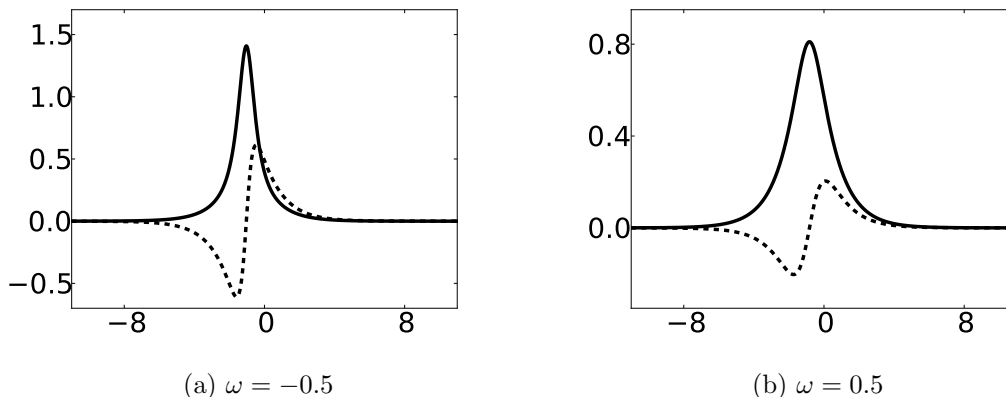


Figure 4: Asymmetric GSs with $V = -U^*$ of (2.2) in the central gap with $\varepsilon = 0.01$, $k = 1$, $\mu = 0.01$ and $\delta = \pi/2$.

unstable manifolds for a three-dimensional Poincaré map in [47]. As detected in the theory, the stable and unstable manifolds are observed to intersect transversely and GSs could be found. The stable and unstable manifolds on the Poincaré section $x = 0 \pmod{2\pi}$ for $\mu = 0$, $\omega = \pm 0.5$, $\varepsilon = 0.01$ and $k = 1$ are drawn in Fig. 2. Intersections of these manifolds give rise to homoclinic orbits or GSs, and symmetric GSs in (2.2) for the same parameter values are plotted in Fig. 3. These GSs are not visibly different from the unperturbed ones of (3.4). In Fig. 4 asymmetric GSs in (2.2) are also plotted for $\mu = 0.01$, $\delta = \pi/2$, $\omega = \pm 0.5$, $\varepsilon = 0.01$ and $k = 1$. Note that there are different asymmetric GSs which have almost the same shapes as those in Fig. 4 but have peaks at a position shifting by π/k . Plots of GSs throughout this paper show the real part of the solutions as a solid curve, whereas the imaginary part is plotted as a dashed curve.

4. Existence of gap solitons in non-central gaps

In order to investigate the existence of GSs of (2.2) with $V = -U^*$ in the non-central gaps, we shall use the higher-order averaging method [28, 29]. Let us describe a general setup for the averaging analysis.

We seek homoclinic solutions to the origin of (3.2) near $\omega = \omega_{\pm m}$ in the limit of small ε, μ . Note that for $\varepsilon = \mu = 0$ the origin is an equilibrium in (3.2), at which the Jacobian matrix has a pair of purely imaginary eigenvalues $\lambda = \pm i\sqrt{\omega^2 - 1}$ when $\omega \approx \omega_{\pm m}$. Let j and l be non-negative integers which will be determined for each gap later. Define a detuning parameter Ω by

$$\varepsilon^{j+1}\Omega = \omega - \omega_{\pm m}.$$

Let

$$\Phi(x) = \begin{pmatrix} \cos \frac{mk}{2}x & -\frac{2(\omega_{\pm m} + 1)}{mk} \sin \frac{mk}{2}x \\ \frac{mk}{2(\omega_{\pm m} + 1)} \sin \frac{mk}{2}x & \cos \frac{mk}{2}x \end{pmatrix},$$

which is the fundamental matrix of the linearization at the origin of the unperturbed system (3.3) with $\omega = \omega_{\pm m}$. Using the transformation

$$\begin{pmatrix} a \\ b \end{pmatrix} = \varepsilon^{(l+1)/2} \Phi(x) \begin{pmatrix} \frac{1}{k} \xi \\ m \\ \frac{1}{2(\omega_{\pm m} + 1)} \eta \end{pmatrix} \quad (4.1)$$

in (3.2), one obtains

$$\begin{pmatrix} \xi'/k \\ (m/2)\eta' / (\omega_{\pm m} + 1) \end{pmatrix} = \varepsilon \Phi^{-1}(x) \begin{pmatrix} [-\varepsilon^j \Omega + \cos kx - \bar{\mu} \cos(kx + \delta) - \frac{3}{2} \varepsilon^l (a^2 + b^2)] b \\ [\varepsilon^j \Omega + \cos kx + \bar{\mu} \cos(kx + \delta) + \frac{3}{2} \varepsilon^l (a^2 + b^2)] a \end{pmatrix}, \quad (4.2)$$

where $\bar{\mu} = \mu/\varepsilon$ and a and b are represented by ξ and η via (4.1).

Homoclinic solutions in (4.2), equivalently in (3.2), can be approximately obtained by the averaging method. These homoclinic solutions correspond to GPs of (2.2) with $V = -U^*$ in the non-central gaps. While in the first gaps $\mathbf{1}^\pm$ the standard (i.e., first-order) averaging method is sufficient, we have to use the higher-order averaging method for the higher-order gaps. This difficulty occurs because the potential considered here consists of the pure harmonic component $\cos kx$. But it is important to note that higher-order averaging is also needed for more general potentials with higher Fourier components, if these higher components are small compared to the first one. This is the reason for us to present the higher-order method here.

The necessary lengthy computations can be easily performed with computer algebra systems. Specifically, we have used the program `haverage.m` for the computer software `Mathematica` [42], developed in [46, 48] (see also [45]). We exemplarily present the results for the first three gaps $\mathbf{1}^\pm$, $\mathbf{2}^\pm$ and $\mathbf{3}^\pm$. Similar second-order averaging analyses can also calculate the boundaries of the central gap (see Appendix B).

4.1. Averaging in the gaps $\mathbf{1}^\pm$

For the computations in the first gap at $\omega_{\pm 1} = \pm \sqrt{1 + k^2/4}$, we set $m = 1$ and $j = l = 0$. The standard averaging procedure for (4.2) yields the first-order averaged system

$$\begin{aligned} \xi' &= \varepsilon \left[-\frac{\bar{\mu} \sin \delta}{k} \xi + \frac{\omega_{\pm 1}(1 - 2\Omega) + \bar{\mu} \cos \delta}{k} \eta - \gamma_{\pm 1}(\xi^2 + \eta^2)\eta \right], \\ \eta' &= \varepsilon \left[\frac{\omega_{\pm 1}(1 + 2\Omega) + \bar{\mu} \cos \delta}{k} \xi + \frac{\bar{\mu} \sin \delta}{k} \eta + \gamma_{\pm 1}(\xi^2 + \eta^2)\xi \right], \end{aligned} \quad (4.3)$$

where

$$\gamma_{\pm 1} = \frac{3(2\omega_{\pm 1}^2 + 1)}{2k^3(\omega_{\pm 1} + 1)^3} > 0.$$

Eqs. (4.3) are easily obtained by averaging the right hand side of (4.2) with respect to x over $[0, 2\pi/k]$ and such computations can be done by the **Mathematica** program `haverage.m`. In the averaged system (4.3) with $\bar{\mu} \cos \delta + \omega_{\pm 1} \neq 0$, we perform a rotational transformation

$$\begin{pmatrix} \tilde{\xi} \\ \tilde{\eta} \end{pmatrix} = \begin{pmatrix} \cos \theta & \sin \theta \\ -\sin \theta & \cos \theta \end{pmatrix} \begin{pmatrix} \xi \\ \eta \end{pmatrix}$$

to obtain a system of a more convenient form

$$\begin{aligned} \tilde{\xi}' &= \varepsilon \left[\frac{2\omega_{\pm 1}}{k} (\Omega_{1\pm} - \Omega) \tilde{\eta} - \gamma_{\pm 1} (\tilde{\xi}^2 + \tilde{\eta}^2) \tilde{\eta} \right], \\ \tilde{\eta}' &= \varepsilon \left[\frac{2\omega_{\pm 1}}{k} (\Omega_{1\pm} + \Omega) \tilde{\xi} + \gamma_{\pm 1} (\tilde{\xi}^2 + \tilde{\eta}^2) \tilde{\xi} \right], \end{aligned} \quad (4.4)$$

where

$$\Omega_{1\pm} = \frac{1}{2} \sqrt{\left(\frac{\bar{\mu}}{\omega_{\pm 1}} \right)^2 + 2 \left(\frac{\bar{\mu}}{\omega_{\pm 1}} \right) \cos \delta + 1}$$

and

$$\theta = \begin{cases} \theta_1 & \text{for } \omega_{\pm 1} (\bar{\mu} \cos \delta + \omega_{\pm 1}) > 0; \\ \theta_1 + \frac{\pi}{2} & \text{for } \omega_{\pm 1} (\bar{\mu} \cos \delta + \omega_{\pm 1}) < 0 \end{cases}$$

with

$$\theta_1 = \frac{1}{2} \arctan \left(\frac{\bar{\mu} \sin \delta}{\bar{\mu} \cos \delta + \omega_{\pm 1}} \right) \in [-\pi, \pi].$$

Note that Eq. (4.4) is still valid for $\bar{\mu} \cos \delta + \omega_{\pm 1} = 0$ if $\theta = \pi/4$ is taken when $\omega_{\pm 1} \bar{\mu} \sin \delta > 0$ and if $\theta = -\pi/4$ is taken when $\omega_{\pm 1} \bar{\mu} \sin \delta < 0$. The system (4.4) is Hamiltonian with a Hamilton function

$$H_1(\tilde{\xi}, \tilde{\eta}) = \varepsilon \left\{ \frac{\omega_{\pm 1}}{k} [(\Omega_{1\pm} + \Omega) \tilde{\xi}^2 - (\Omega_{1\pm} - \Omega) \tilde{\eta}^2] + \frac{1}{4} \gamma_{\pm 1} (\tilde{\xi}^2 + \tilde{\eta}^2)^2 \right\},$$

for which the origin $(\tilde{\xi}, \tilde{\eta}) = (0, 0)$ is a saddle if $\Omega \in (-\Omega_{1\pm}, \Omega_{1\pm})$, i.e.,

$$\omega \in (\omega_{\pm 1} - \varepsilon \Omega_{1\pm}, \omega_{\pm 1} + \varepsilon \Omega_{1\pm}). \quad (4.5)$$

We easily see that if

$$\mu = \varepsilon \sqrt{1 + \frac{1}{4} k^2}, \quad \delta = 0 \quad (\text{resp. } \delta = \pi) \quad (4.6)$$

then $\Omega_{1+} = 0$ (resp. $\Omega_{1-} = 0$) and a closing of the gap region $\mathbf{1}^+$ (resp. $\mathbf{1}^-$) occurs. See also Fig. 1(d). If $\delta \neq 0, \pi$, then $\Omega_{1\pm} \neq 0$, and thus such a closing does not occur.

Let us assume that $\Omega_{1\pm} \neq 0$, i.e., condition (4.6) does not hold. A straightforward analysis of the level sets of H_1 shows the existence of two homoclinic orbits in (4.4) and hence in (4.3). Moreover, we can obtain

analytical expressions of the homoclinic orbits as

$$\begin{aligned}
& (\tilde{\xi}_{\pm}(x), \tilde{\eta}_{\pm}(x)) \\
&= \left(\pm 2 \sqrt{\frac{2\omega_{\pm 1}\Omega_{1\pm}}{3k\gamma_{\pm 1}}} \sin \phi \sin \frac{1}{2} \phi \frac{\sinh[(2\omega_{\pm 1}\Omega_{1\pm} \sin \phi/k)\varepsilon x]}{\cosh[(4\omega_{\pm 1}\Omega_{1\pm} \sin \phi/k)\varepsilon x] + \cos \phi}, \right. \\
&\quad \left. \mp 2 \sqrt{\frac{2\omega_{\pm 1}\Omega_{1\pm}}{3k\gamma_{\pm 1}}} \sin \phi \cos \frac{1}{2} \phi \frac{\cosh[(2\omega_{\pm 1}\Omega_{1\pm} \sin \phi/k)\varepsilon x]}{\cosh[(4\omega_{\pm 1}\Omega_{1\pm} \sin \phi/k)\varepsilon x] + \cos \phi} \right), \tag{4.7}
\end{aligned}$$

where $\Omega/\Omega_{1\pm} = \cos \phi$.

It is easy to see that, since the coefficient in front of $\tilde{\eta}^2$ in H_1 is negative, the homoclinic orbits intersect the $\tilde{\eta}$ -axis and are symmetric about it, forming a figure-of-eight configuration. In general, it is very difficult to make precise statements about the symmetry of homoclinic orbits in (4.3). For some special cases, however, we have the following results:

- (i) When $\bar{\mu} > 0$ and $\delta = 0$, the homoclinic orbits in the averaged system (4.3) are symmetric about the η -axis if $\bar{\mu} < -\omega_{\pm 1}$ and about the ξ -axis if $\bar{\mu} > -\omega_{\pm 1}$ in the negative gap, while they are always symmetric about the η -axis in the positive gap.
- (ii) When $\mu > 0$ and $\delta = \pi$, the homoclinic orbits in (4.3) are symmetric about the η -axis if $\bar{\mu} < \omega_{\pm 1}$ and about the ξ -axis if $\bar{\mu} > \omega_{\pm 1}$ in the positive gap, while they are always symmetric about the η -axis in the negative gap.
- (iii) When $\mu = 0$, the homoclinic orbits in (4.3) are symmetric about the η -axis in both the positive and negative gaps.

From the existence of homoclinic orbits in the averaged system (4.3), we claim that there exist homoclinic orbits in (3.1) and hence stationary GSs in (2.2). For this consider (4.2) and (4.3) as dynamical systems defined in the phase space $\mathbb{R}^2 \times \mathbb{S}^1$. Recall that we set $m = 1$ and $j = l = 0$ in (4.2). We introduce a cross section Σ at $x = 0 \pmod{2\pi/k}$ and define the Poincaré maps $\psi, \bar{\psi} : \Sigma \rightarrow \Sigma$ for (4.2) and (4.3), respectively. For both ψ and $\bar{\psi}$ the origin $(\xi, \eta) = (0, 0)$ is a fixed point and has stable and unstable manifolds. Moreover, the stable and unstable manifolds, $\bar{W}^s(0)$ and $\bar{W}^u(0)$, coincide along the homoclinic orbits in (4.3) for $\bar{\psi}$. By the averaging theorem (see Theorem 4.1.1 of [17]), the stable and unstable manifolds, $W^s(0)$ and $W^u(0)$, for ψ are $O(\varepsilon)$ -close to $\bar{W}^s(0)$ and $\bar{W}^u(0)$. Since Eq. (4.2) as well as Eq. (4.3) are Hamiltonian, the Poincaré maps $\psi, \bar{\psi}$ are area-preserving.

Now assume that the stable and unstable manifolds $W^s(0)$ and $W^u(0)$ do not intersect, and go inward and outward, respectively, as shown in Fig. 5. We want to show that this yields a contradiction and define a region S , which is encircled by two parts of $W^s(0)$ and $W^u(0)$ and a line connecting two points p_1 and p_2 on $W^s(0)$ and $W^u(0)$. The region S is mapped by the Poincaré map ψ to another region $S' = \psi(S)$ which is encircled by two different parts of $W^s(0)$ and $W^u(0)$ and a curve connecting two points $\psi(p_1)$ and $\psi(p_2)$ on

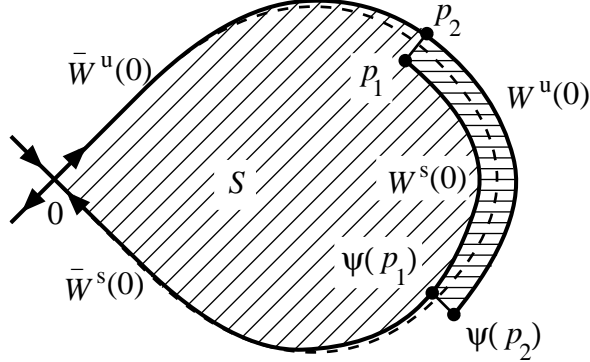


Figure 5: Stable and unstable manifolds $W^{s,u}(0)$ (solid lines) which are close to $\bar{W}^{s,u}(0)$ (broken lines) but do not intersect. The regions S and $S' \setminus S$ with $S' = \psi(S)$ are hatched distinctly.

$W^s(0)$ and $W^u(0)$. It is obvious that S' is larger than S and contradicts the fact that ψ is area-preserving. Similarly, we cannot assume that $W^s(0)$ and $W^u(0)$ go outward and inward, respectively. Therefore, we can prove that $W^s(0)$ and $W^u(0)$ intersect and there exists a homoclinic orbit in the full system (4.2) and hence in (3.1). On the other hand, Eq. (4.2) can be averaged up to $O(\varepsilon^n)$ for any integer $n \geq 1$ but has very rapid oscillations compared with the unperturbed homoclinic orbits (4.7) which vary very slowly with $O(1/\varepsilon)$. Applying a result by Neishtadt [30] (see also [40]), we see that the splitting distance between $W^s(0)$ and $W^u(0)$ is exponentially small with respect to ε at most. Thus, there exist stationary GS solutions to the system of equations (2.2) in the gap regions (4.5).

Moreover, assume that $\mu \sin \delta = 0$, i.e., $\mu = 0$ or $\delta = 0, \pi$, so that Eqs. (3.2) is reversible with respect to R_j and R'_j , $j = 1, 2$. Then it follows from the above arguments that the homoclinic orbit in the averaged system (4.3) is symmetric about the ξ -axis (resp. η -axis). By the persistence of symmetric orbits in reversible systems, there exist symmetric homoclinic orbits about the ξ -axis (resp. η -axis) in the full system (4.2) and with respect to R_1 and R'_1 (resp. R_2 and R'_2) in (3.2) and hence in (3.1). In particular, the homoclinic orbits in (3.1) have an even (resp. odd) real part a and odd (resp. even) imaginary part b .

We can use similar arguments to the central gap when condition (3.8) does not hold, and prove that there must be homoclinic orbits. However, the splitting distance between the stable and unstable manifolds is not exponentially small with respect to ε but $O(\varepsilon^2)$ at most since both of the perturbations in (3.2) and unperturbed homoclinic orbits (3.4) vary with $O(1)$.

In addition, we can detect a non-transverse homoclinic orbit in (3.2) when $\delta = \pi$ and

$$\varepsilon \approx \varepsilon_0 = \frac{2\mu}{k} \tanh\left(\frac{k\theta}{2\sin\theta}\right), \quad (4.8)$$

as follows. Fix $\delta = \pi$. Then the Melnikov functions $M_{\pm}(x_0)$ have graphs as shown in Fig. 6, depending on

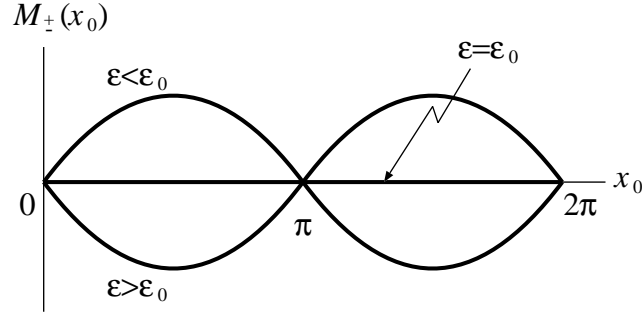


Figure 6: Graphs of the Melnikov functions $M_{\pm}(x_0)$ for $\delta = \pi$.

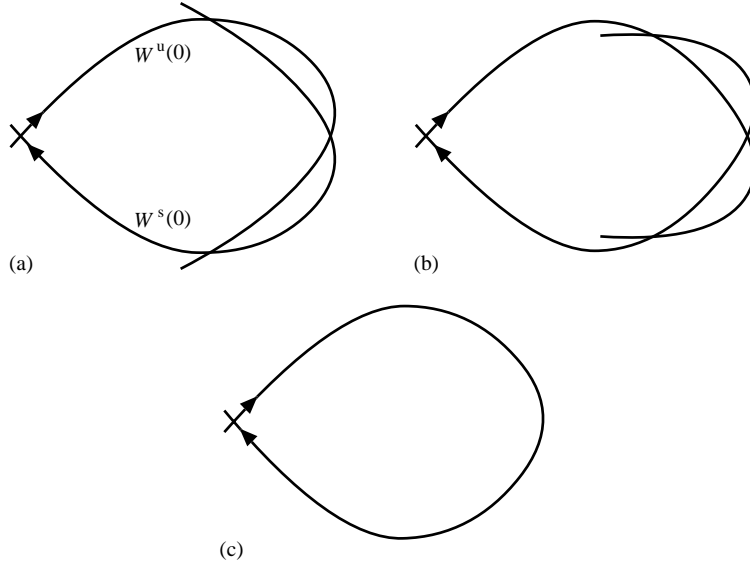


Figure 7: Stable and unstable manifolds $W^{s,u}(0)$ for the associated Poincaré map: (a) $\varepsilon < \varepsilon_0$; (b) $\varepsilon > \varepsilon_0$; (c) $\varepsilon = \varepsilon_0$.

$\varepsilon < \varepsilon_0$, $\varepsilon = \varepsilon_0$ or $\varepsilon > \varepsilon_0$. Since $M_{\pm}(x_0)$ represent signed measures of their distance (see, e.g., section 4.5 of [41]), noting that $b_{\pm}(x_0) = 0$ and Eqs. (3.2) is reversible, we can draw the behavior of the stable and unstable manifolds $W^{s,u}(0)$ for the Poincaré map of (3.2) as shown in Figs. 7(a) and (b). Using the fact that the Poincaré map is area-preserving and applying a discussion similar to the above one for (4.2), we see that $W^s(0)$ and $W^u(0)$ coincide for some ε near ε_0 , say $\tilde{\varepsilon}_0$, as shown in Fig. 7(c). Thus, the point $(\delta, \varepsilon) = (\pi, \tilde{\varepsilon}_0)$ is very degenerate in the parameter space. This also suggests that new interesting behavior may occur at the point in the original PDEs (2.2).

In Fig. 8 we show the results of numerical computations of the stable and unstable manifolds by AUT097 with HomMap near the homoclinic bifurcation point $\varepsilon = \varepsilon_0 \approx 0.010806$ for $\mu = 0.01$, $\omega = 0.5$ and $k = 1$.

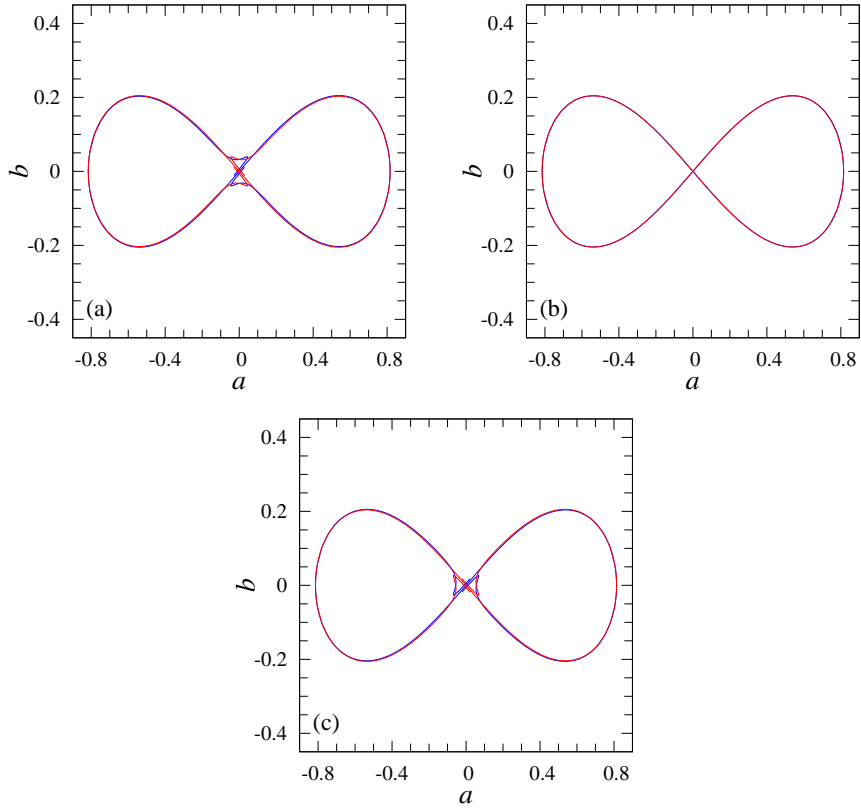


Figure 8: Stable and unstable manifolds of the origin on the Poincaré section $x = 0 \pmod{2\pi}$ when $\mu = 0.01$, $\omega = 0.5$, $\delta = \pi$ and $k = 1$: (a) $\varepsilon = 0.0088063$; (b) $\varepsilon = 0.0108063$; (c) $\varepsilon = 0.0128063$. The red and blue curves represent the stable and unstable manifolds, respectively.

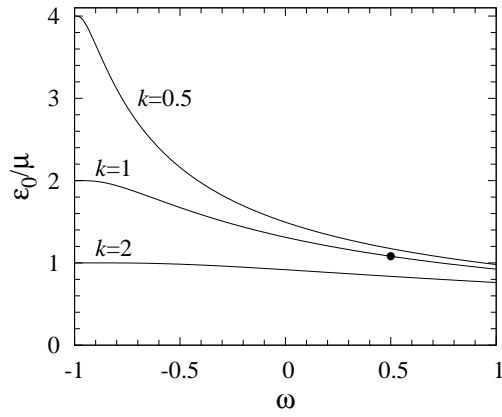


Figure 9: Homoclinic bifurcation curves for Eqs. (3.2) with $k = 0.5, 1, 2$. The parameter values (ω, ε) of Fig. 8(b) with $k = 1$ is plotted as \bullet .

We see that as predicted by the theory, the invariant manifolds almost coincide at $\varepsilon \approx \varepsilon_0$ while they split when ε is different from ε_0 . Thus, the theoretical prediction for the homoclinic bifurcations is very precise. Figure 9 also shows the approximate homoclinic bifurcation curves given by Eq. (4.8), on which the stable and unstable manifolds coincide, in the $(\omega, \varepsilon/\mu)$ -space for $k = 0.5, 1, 2$.

4.2. Averaging in the gaps 2^\pm

We set $m = 2$ and $j = l = 1$, and perform a second-order averaging method to prove the existence of gap solitons of (2.3) with $V = -U^*$ in the second gaps appearing at $\omega_{\pm 2} = \pm\sqrt{1+k^2}$. To avoid the complexity of expressions, we give our results only for $\mu = 0$ in the gaps of higher orders. The second-order averaged system has been obtained using the *Mathematica* program `haverage.m`, and it reads

$$\begin{aligned}\xi' &= -\frac{\varepsilon^2}{k^2} \left\{ \alpha_{\pm 2} \left[(6(\omega_{\pm 2} + 1)\Omega - 5)k^2 + (\omega_{\pm 2} + 1)^2 \right] \right. \\ &\quad \left. + \beta_{\pm 2} \left[k^2\xi^2 + (\omega_{\pm 2} + 1)^2\eta^2 \right] \right\} \eta, \\ \eta' &= \frac{\varepsilon^2}{(\omega_{\pm 2} + 1)^2} \left\{ \alpha_{\pm 2} \left[(6(\omega_{\pm 2} + 1)\Omega + 1)k^2 - 5(\omega_{\pm 2} + 1)^2 \right] \right. \\ &\quad \left. + \beta_{\pm 2} \left[k^2\xi^2 + (\omega_{\pm 2} + 1)^2\eta^2 \right] \right\} \xi,\end{aligned}\tag{4.9}$$

with

$$\begin{aligned}\alpha_{\pm 2} &= \frac{k^2 + (\omega_{\pm 2} + 1)^2}{12k^2(\omega_{\pm 2} + 1)}, \\ \beta_{\pm 2} &= \frac{3[3k^4 + 2(\omega_{\pm 2} + 1)^2k^2 + 3(\omega_{\pm 2} + 1)^4]}{16k^2(\omega_{\pm 2} + 1)^2}.\end{aligned}$$

Note that $\alpha_{+2} = -\alpha_{-2} > 0$ and $\beta_{\pm 2} > 0$. Eq. (4.9) is a Hamiltonian system with the Hamilton function

$$\begin{aligned}H_2(\xi, \eta) &= \varepsilon^2 \left(\frac{\alpha_{\pm 1/1} \{ [6(\omega_{\pm 1/1} + 1)\Omega + 1]k^2 - 5(\omega_{\pm 1/1} + 1)^2 \}}{2(\omega_{\pm 1/1} + 1)^2} \xi^2 \right. \\ &\quad \left. + \frac{\alpha_{\pm 1/1} \{ [6(\omega_{\pm 1/1} + 1)\Omega - 5]k^2 + (\omega_{\pm 1/1} + 1)^2 \}}{2k^2} \eta^2 \right. \\ &\quad \left. + \frac{\beta_{\pm 1/1}}{4k^2(\omega_{\pm 2/1} + 1)^2} [k^2\xi^2 + (\omega_{\pm 1/1} + 1)^2\eta^2]^2 \right).\end{aligned}$$

Let

$$\begin{aligned}\Delta\Omega_2^1 &= \frac{2k^2 - \sqrt{k^2 + 1} - 1}{3k^2(\sqrt{k^2 + 1} + 1)} = \frac{2k^2 - 5\sqrt{k^2 + 1} + 5}{3k^2(\sqrt{k^2 + 1} - 1)}, \\ \Delta\Omega_2^2 &= \frac{2k^2 + 5\sqrt{k^2 + 1} + 5}{3k^2(\sqrt{k^2 + 1} + 1)} = \frac{2k^2 + \sqrt{k^2 + 1} - 1}{3k^2(\sqrt{k^2 + 1} - 1)}.\end{aligned}$$

The origin is a saddle of (4.9) and has a pair of homoclinic orbits if $\Omega \in (\Delta\Omega_2^1, \Delta\Omega_2^2)$ and $\Omega \in (-\Delta\Omega_2^2, -\Delta\Omega_2^1)$ when the signs ‘+’ and ‘-’ are taken in the subscript of ω in (4.9), respectively, i.e.,

$$\omega \in (\omega_{+2} + \varepsilon^2\Delta\Omega_2^1, \omega_{+2} + \varepsilon^2\Delta\Omega_2^2)$$

or

$$\omega \in (\omega_{-2} - \varepsilon^2 \Delta \Omega_2^2, \omega_{-2} - \varepsilon^2 \Delta \Omega_2^1).$$

Again, we find the averaged system to be Hamiltonian with a saddle equilibrium at the origin, and a study of the corresponding level set of the Hamiltonian shows the existence of a figure-of-eight of homoclinic orbits. These orbits intersect the η -axis. By the same argument as above, this implies the existence of gap solitons for (3.1) in the gaps $\mathbf{2}^\pm$ having an even a -component and an odd b -component.

4.3. Averaging in the gaps $\mathbf{3}^\pm$

We set $m = 3$, $j = 1$ and $l = 2$, and perform the third-order averaging procedure for (4.2) using the `Mathematica` program `haverage.m` to obtain the averaged system

$$\begin{aligned} \xi' &= -\frac{\varepsilon^2}{9k^2} \rho_{\pm 3} \{ [32(\omega_{\pm 3} + 1)\Omega - 9]k^2 - 4(\omega_{\pm 3} + 1)^2 \} \eta \\ &\quad + \frac{\varepsilon^3}{9k^2} \{ \alpha_{\pm 3} - \beta_{\pm 3} [9k^2 \xi^2 + 4(\omega_{\pm 3} + 1)^2 \eta^2] \} \eta, \\ \eta' &= \frac{\varepsilon^2}{4(\omega_{\pm 3} + 1)^2} \rho_{\pm 3} \{ [32(\omega_{\pm 3} + 1)\Omega - 9]k^2 - 4(\omega_{\pm 3} + 1)^2 \} \xi \\ &\quad + \frac{\varepsilon^3}{4(\omega_{\pm 3} + 1)^2} \{ \alpha_{\pm 3} + \beta_{\pm 3} [9k^2 \xi^2 + 4(\omega_{\pm 3} + 1)^2 \eta^2] \} \xi, \end{aligned} \tag{4.10}$$

where

$$\begin{aligned} \rho_{\pm 3} &= \frac{9k^2 + 4(\omega_{\pm 3} + 1)^2}{64k^2(\omega_{\pm 3} + 1)}, \\ \alpha_{\pm 3} &= \frac{3[9k^2 + 4(\omega_{\pm 3} + 1)^2][81k^4 - 56(\omega_{\pm 3} + 1)^2k^2 + 16(\omega_{\pm 3} + 1)^4]}{512k^4(\omega_{\pm 3} + 1)^2}, \\ \beta_{\pm 3} &= \frac{81k^4 + 24(\omega_{\pm 3} + 1)^2k^2 + 16(\omega_{\pm 3} + 1)^4}{64k^2(\omega_{\pm 3} + 1)^2}. \end{aligned}$$

Note that $\rho_{+3} = -\rho_{-3} > 0$ and $\alpha_{\pm 3}, \beta_{\pm 3} > 0$ since

$$\begin{aligned} &81k^4 - 56(\omega_{\pm 3} + 1)^2k^2 + 16(\omega_{\pm 3} + 1)^4 \\ &= [9k^2 - 4(\omega_{\pm 3} + 1)^2]^2 + 18(\omega_{\pm 3} + 1)^2 > 0. \end{aligned}$$

Let

$$\Omega = \Omega_{\pm 3} + \varepsilon\nu,$$

where

$$\Omega_{\pm 3} = \frac{9k^2 + 4(\omega_{\pm 3} + 1)^2}{32(\omega_{\pm 3} + 1)k^2}.$$

Note that $\Omega_{+3} > 0$ and $\Omega_{-3} < 0$. Eq. (4.10) becomes

$$\begin{aligned} \xi' &= -\frac{\varepsilon^3}{9k^2} \{ (\gamma_{\pm 3}\nu - \alpha_{\pm 3}) + \beta_{\pm 3}[9k^2 \xi^2 + 4(\omega_{\pm 3} + 1)^2 \eta^2] \} \eta, \\ \eta' &= \frac{\varepsilon^3}{4(\omega_{\pm 3} + 1)^2} \{ (\gamma_{\pm 3}\nu + \alpha_{\pm 3}) + \beta_{\pm 3}[9k^2 \xi^2 + 4(\omega_{\pm 3} + 1)^2 \eta^2] \} \xi, \end{aligned} \tag{4.11}$$

where

$$\gamma_{\pm 3} = 32\rho_{\pm 3}(\omega_{\pm 3} + 1)k^2 = \frac{1}{2}[9k^2 + 4(\omega_{\pm 3} + 1)^2] > 0.$$

Eq. (4.11) is a Hamiltonian system with the Hamilton function

$$H_3(\xi, \eta) = \varepsilon^3 \left(\frac{\gamma_{\pm 3}\nu + \alpha_{\pm 3}}{8(\omega_{\pm 3} + 1)^2} \xi^2 + \frac{\gamma_{\pm 3}\nu - \alpha_{\pm 3}}{18k^2} \eta^2 + \frac{\beta_{\pm 3}}{144k^2(\omega_{\pm 2/1} + 1)^2} [9k^2\xi^2 + 4(\omega_{\pm 2/1} + 1)^2\eta^2]^2 \right). \quad (4.12)$$

We easily see that

$$\frac{\alpha_{+3}}{\gamma_{+3}} = \frac{\alpha_{-3}}{\gamma_{-3}} = \frac{3(k^4 + 4)}{16k^4}$$

and set

$$\Delta\Omega_3 = \frac{3(k^4 + 4)}{16k^4}.$$

The origin is a saddle and has a pair of homoclinic orbits if $\nu \in (-\Delta\Omega_3, \Delta\Omega_3)$, i.e.,

$$\omega \in (\omega_{\pm 3} \pm \varepsilon^2\Omega_3 - \varepsilon^3\Delta\Omega_3, \omega_{\pm 3} \pm \varepsilon^2\Omega_3 + \varepsilon^3\Delta\Omega_3).$$

Especially, in the regions (4.3) the coefficients of ξ^2 and η^2 in the Hamiltonian (4.12) are positive and negative, respectively, so that the pair of homoclinic orbits draws a vertical figure-eight' in the (ξ, η) -phase plane.

Similar computations reveal the existence of gap solitons in the higher order gaps. These solutions are odd in a (and even in b) or vice versa, depending on whether the gap number is odd or even. A general proof of this is beyond the scope of this paper. In the following we illustrate and extend this perturbative results by numerical computations.

4.4. Numerical studies

We computed the stable and unstable manifolds of the origin and homoclinic orbits in (3.2), i.e., GSs with $V = -U^*$ in (2.2), using the computer package, AUTO with HomMap. In our computations we found GSs due to the transverse intersection of the stable and unstable manifolds, thus confirming the analytical results. For several parameter values, the stable and unstable manifolds for the Poincaré section $x = 0 \pmod{2\pi}$ are shown in Fig. 10 and GSs in (2.2) are plotted in Figs. 11-13. In addition to the solutions of (3.2), the figures include homoclinic solutions of the averaged systems (4.3), (4.9) and (4.11), rescaled according to the transformation (4.1). As can be seen, they provide a good match to the envelope of the solutions to (3.2). In all figures presented, the parameter k has been set to $k = 1$.

In closing this section, we return to the parameter values of Fig. 1(d). In this case a new bandgap opens up for small ε , but closes at $\varepsilon = 1/\sqrt{8}$. See also formula (4.6). Our computations reveal that GSs exist in the gaps both above and below this parameter value. In Fig. 14 we show solution profiles at $\varepsilon = 0.2$ and $\varepsilon = 0.8$.

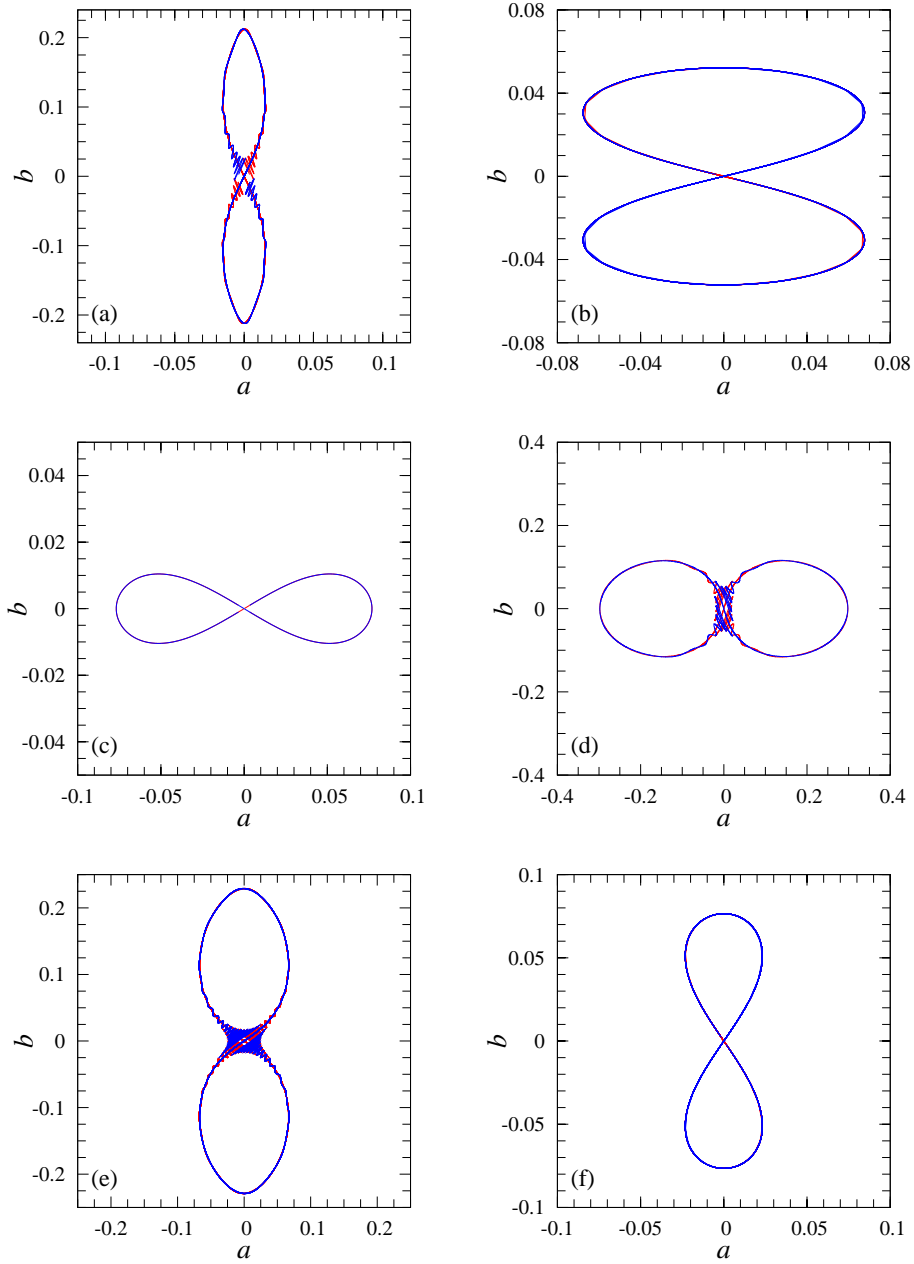


Figure 10: Stable and unstable manifolds of the origin on the Poincaré section $x = 0 \bmod 2\pi$ when $\mu = 0$ and $k = 1$: (a) $\omega = -1.118$, $\varepsilon = 0.045$; (b) $\omega = 1.118$, $\varepsilon = 0.045$; (c) $\omega = -1.42$, $\varepsilon = 0.4$; (d) $\omega = 1.42$, $\varepsilon = 0.4$; (e) $\omega = -1.9$, $\varepsilon = 0.6$; (f) $\omega = 1.9$, $\varepsilon = 0.6$. The red and blue curves represent the stable and unstable manifolds, respectively.

5. Bifurcation of solitons

We further discuss the behavior of GSs under variation of the system parameters. When the parameter values are varied, homoclinic tangencies, i.e., homoclinic bifurcations, can occur, leading to the creation of

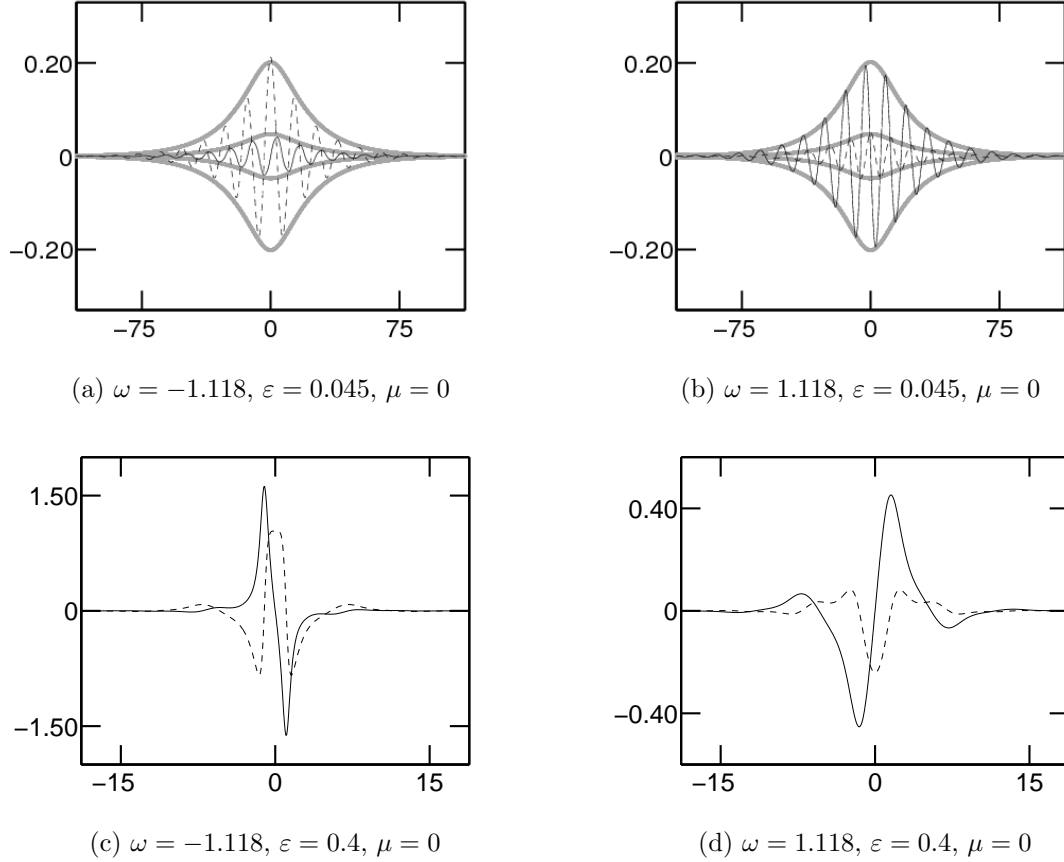


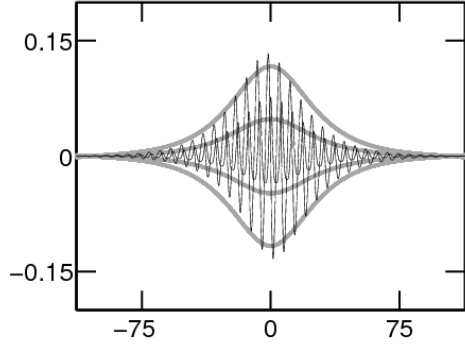
Figure 11: GSs with $V = -U^*$ of (2.3) in the gaps $\mathbf{1}^\pm$, $\mathbf{2}^\pm$ and $\mathbf{3}^\pm$ for $k = 1$, symmetric with respect to R_1 or R_2 . Gray curves in the panels correspond to solutions of the associated averaged system, (4.3), (4.9) or (4.11).

additional GSs and bifurcations of GSs. We have found such bifurcations in all gap regions including the central one.

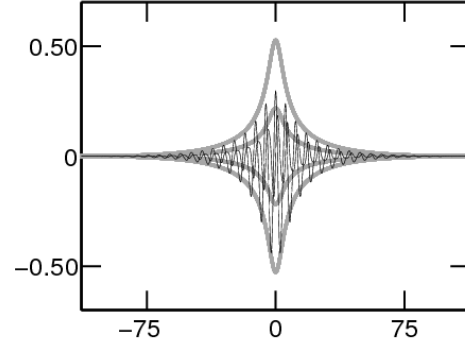
As an example, we plot bifurcation diagrams of GSs for Eqs. (2.3) in the gaps $\mathbf{1}^-$ and $\mathbf{0}$ when $\omega = -1.118$ or 0.5 and $\delta = \pi/2$, in Fig. 15. Here $(a(0), b(0))$ represents the point at which each GS crosses the section $\Sigma = \{x = 0 \text{ mod } 2\pi\}$. In the diagrams we observe saddle-node and pitchfork bifurcations of GSs. The occurrence of these bifurcations is explained from the behavior of the Poincaré map of (3.2) for the section Σ , as follows.

Let us first assume that $\mu \neq 0$, such that the Poincaré map is not reversible. In this case, a tangency between the stable and unstable manifolds as shown in Fig. 16(a) leads to a saddle-node bifurcation, in which two new GSs are created. See Fig. 15(c) for a numerical evidence.

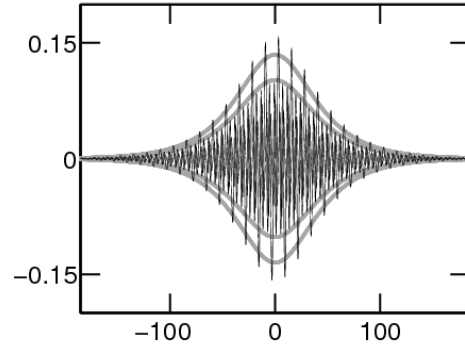
Now suppose that $\mu = 0$ and let us choose a cross-section, such that the Poincaré map is reversible with respect to R_1 and R_2 . We can distinguish two different bifurcation scenarios.



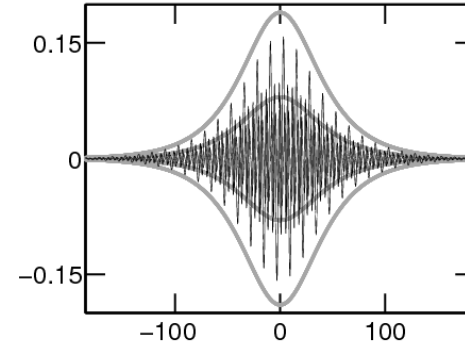
(e) $\omega = -1.42, \varepsilon = 0.4, \mu = 0$



(f) $\omega = 1.42, \varepsilon = 0.4, \mu = 0$

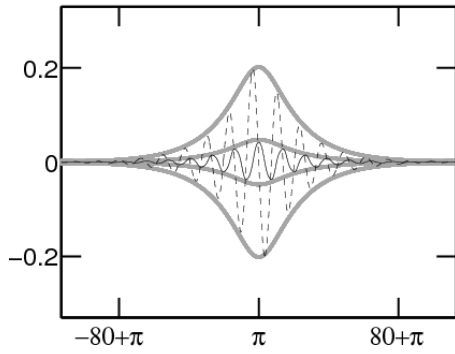


(g) $\omega = -1.9, \varepsilon = 0.6, \mu = 0$

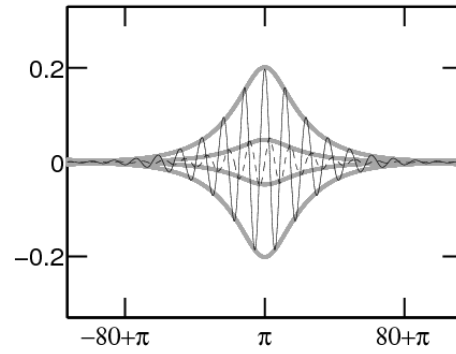


(h) $\omega = 1.9, \varepsilon = 0.6, \mu = 0$

Figure 11: Continued.



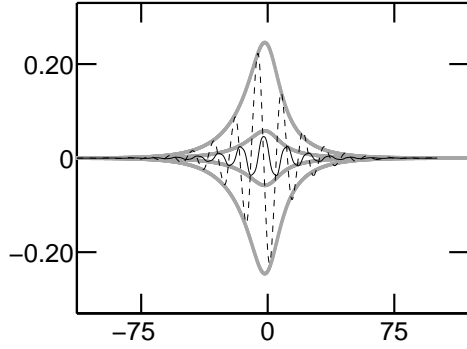
(a) $\omega = -1.118, \varepsilon = 0.045, \mu = 0$



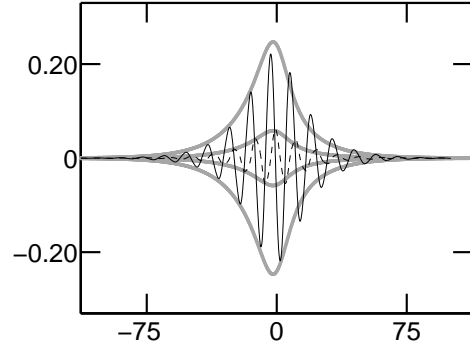
(b) $\omega = 1.118, \varepsilon = 0.045, \mu = 0$

Figure 12: GSs with $V = -U^*$ of (2.3) in the gaps 1^\pm for $k = 1$, symmetric with respect to R'_1 or R'_2 . Gray curves in the panels correspond to solutions of the averaged system (4.3).

If the stable and unstable manifolds have a cubic tangency on the invariant plane of R_1 or R_2 , but intersect

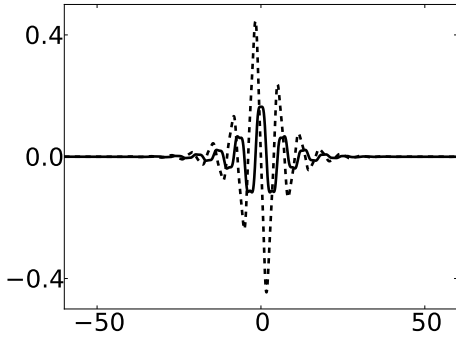


(a) $\omega = -1.118$, $\varepsilon = 0.045$, $\mu = 0.045$, $\delta = \pi/2$

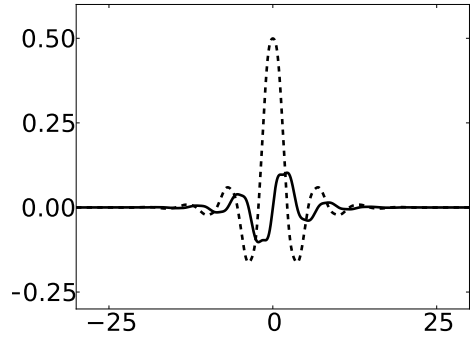


(b) $\omega = 1.118$, $\varepsilon = 0.045$, $\mu = 0.045$, $\delta = \pi/2$

Figure 13: Asymmetric GSs with $V = -U^*$ of (2.3) in the gaps $\mathbf{1}^\pm$ for $k = 1$. Gray curves in the panels correspond to solutions of the averaged system (4.3).



(a) $\varepsilon = 0.2$



(b) $\varepsilon = 0.8$

Figure 14: Symmetric GSs with $V = -U^*$ of (2.3) in the gaps $\mathbf{1}^\pm$ for $\omega = -1.4$, $\mu = 0.5$, $\delta = 0$ and $k = 2$.

this plane transversely as shown in Fig. 16(b), then a pitchfork bifurcation of homoclinic orbits takes place. When the parameters are varied, a pair of homoclinic orbits appear, while the original homoclinic orbit still exists due to the persistence of symmetric orbits. See Figs. 15(a) and (b). The original GS is symmetric, but the two new orbits are asymmetric.

On the other hand, if the stable and unstable manifolds are tangent to the invariant plane at their quadratic tangency as shown in Fig. 16(c), then a saddle-node bifurcation of symmetric GSs occurs. See Fig. 15(b). Note that a saddle-node bifurcation of asymmetric GSs can occur even though $\mu = 0$.

We illustrate these general ideas with computations for equation (3.2). Figure 17 shows the stable and unstable manifolds of the Poincaré map of (3.2) on the section Σ for the parameter values when saddle-node or pitchfork bifurcations occur in Figs. 15.

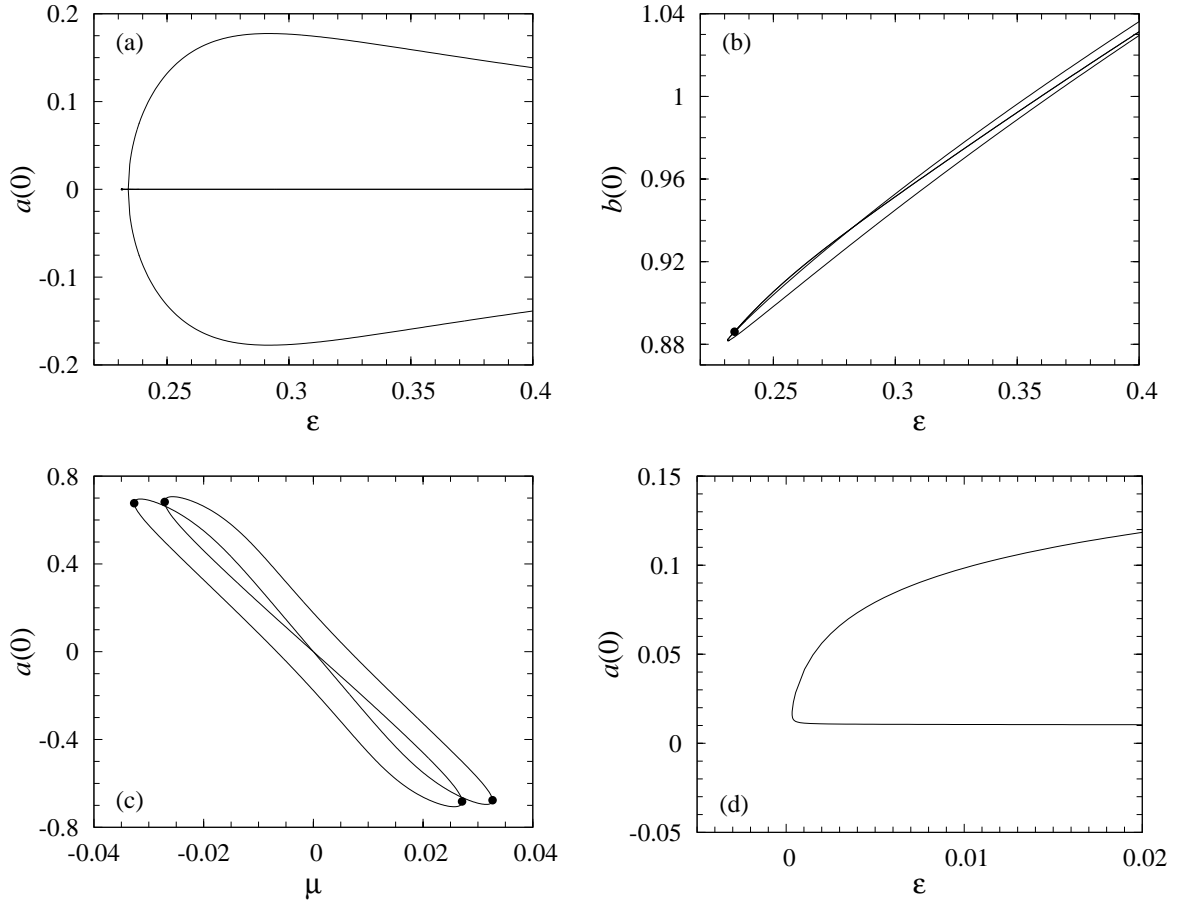


Figure 15: Bifurcation diagrams of GSs in Eqs. (2.3) in the gaps 1^- and 0 for $k = 1$ and $\delta = \pi/2$: (a) and (b) $\omega = -1.118$, $\mu = 0$; (c) $\omega = -1.118$, $\varepsilon = 0.3$; (d) $\omega = 0.5$, $\mu = 0$. In plates (b) and (c), the point “•” represents pitchfork and saddle-node bifurcations, respectively

Figure 17(a) corresponds to Fig. 16(a) and depicts the situation when the map is not reversible ($\mu > 0$) and the stable and unstable manifolds have a quadratic tangency. Similarly, in Figs. 17(b) and (c) the Poincaré map is reversible, and the manifolds have cubic and quadratic tangencies on the invariant plane $b = 0$ as in the sketches in Figs. 16(b) and (c).

Figures 18 and 19 show the profiles of GSs born at the bifurcations in Figs. 15(a)-(c) and (d), respectively. In particular, the GSs in Fig. 19 are bound states with two humps. Standard results about transverse homoclinic orbits explain the existence of multi-pulse GSs, see [41], and we also find such GSs in the other gap regions.

We note that bifurcations of symmetric homoclinic orbits in reversible systems that are *autonomous* have been discussed in [6, 22]. Our analysis of the Poincaré map also yields comparable bifurcation results in systems with periodic forcing like Eqs. (3.2).

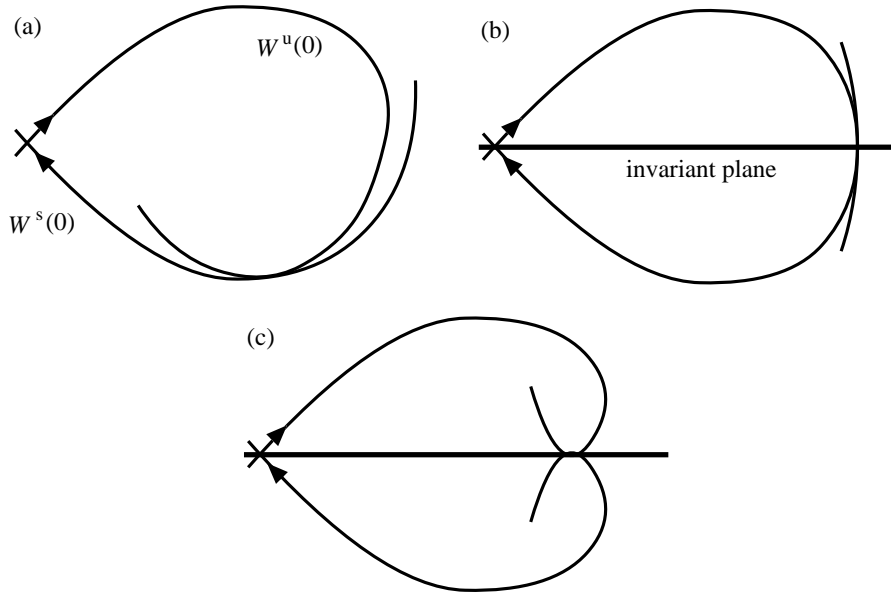


Figure 16: Homoclinic bifurcations in the Poincaré map. Panel (a) depicts the situation that leads to a saddle-node bifurcation of asymmetric GSs. Panels (b) and (c), respectively, explain mechanisms for pitchfork and saddle-node bifurcations of symmetric GSs.

6. Conclusions

In this paper we have studied the existence of GSs (gap solitons) in a model of the BG (Bragg grating) subjected to periodic modulation along the fiber, thus creating the supergrating. The corresponding mathematical model amounts to a parametrically forced extension of the standard BG model with the additional symmetry-breaking forcing term.

As was known previously [5], the supergrating opens up a set of new bandgaps. Using the Melnikov method and averaging techniques, we have demonstrated that families of GSs exist robustly in the new gaps. We have also analyzed bifurcations of GSs and showed that, in addition to the fundamental GSs, the model also supports families of bound states of the solitons.

Many of the GSs found in the model are completely stable, as was verified by means of direct simulations for some of them [49]. The present paper extends the results of [49] and gives detailed mathematical proofs for them, although we did not analyze the stability problem here in detail. In particular, we have discussed the effects of the symmetry-breaking forcing term and demonstrated that it can lead to the closing and re-opening of the bandgaps. In the presence of the new term, GSs exist robustly (as generic solutions) in all the bandgaps, but, as the symmetry of the equation is broken, they undergo many bifurcations.

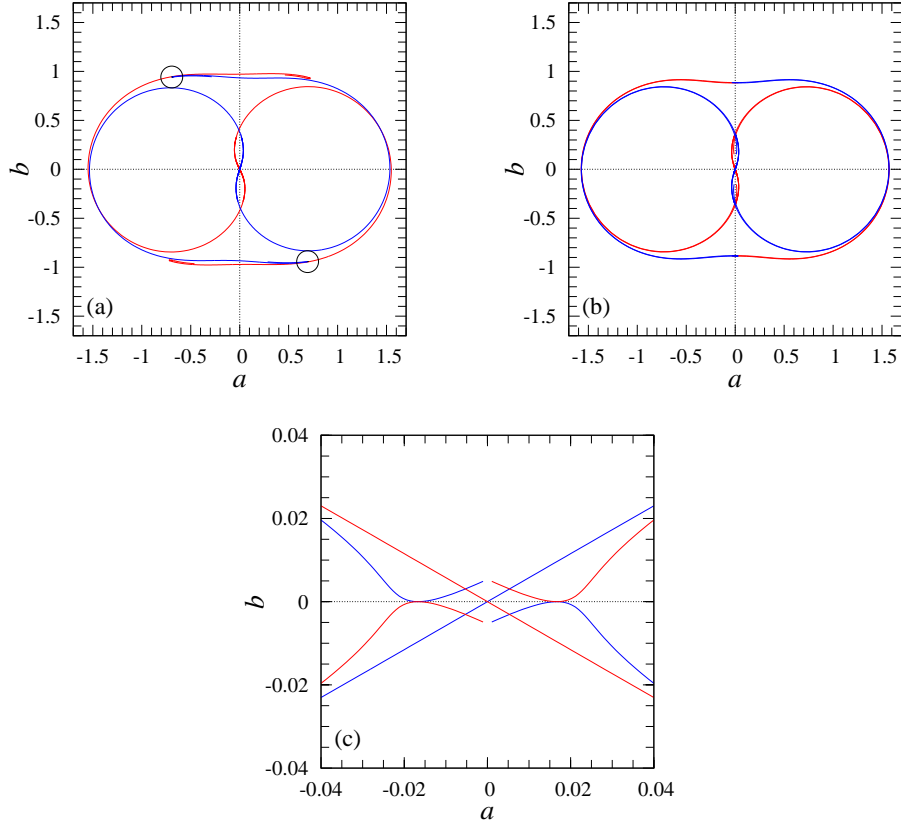


Figure 17: Stable and unstable manifolds of the origin on the Poincaré section $x = 0 \pmod{2\pi}$ when $k = 1$ and $\delta = \pi/2$: (a) $\omega = -1.118, \varepsilon = 0.3, \mu = 0.0326551$; (b) $\omega = -1.118, \varepsilon = 0.234076, \mu = 0$; (c) $\omega = 0.5, \varepsilon = 3.35338 \times 10^{-4}, \mu = 0$. The red and blue curves represent the stable and unstable manifolds, respectively. In plate (a) the invariant manifolds have quadratic tangencies inside the circles.

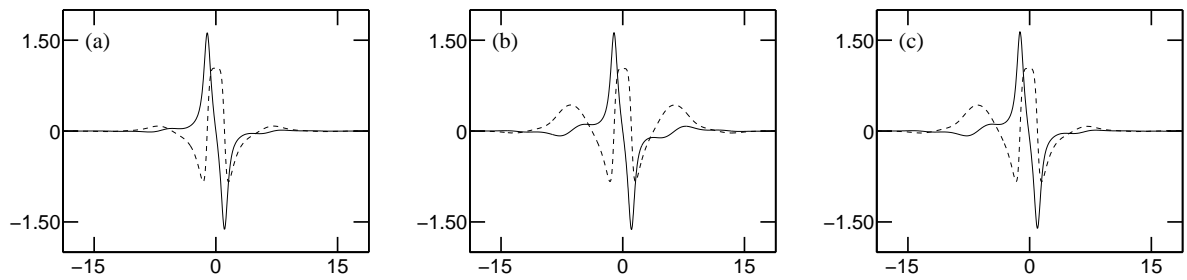


Figure 18: GSs with $V = -U^*$ of (2.3) born at the bifurcations of Fig. 15(a)-(c) for $\varepsilon = 0.4, \omega = -1.118, k = 1$ and $\mu = 0$. The GSs in plates (a) and (b) are symmetric and born at the saddle-node bifurcation while the GSs in plate (c) is asymmetric and born at the pitchfork bifurcation.

Acknowledgments

This research was initiated and many important parts were carried out when the authors worked with Alan Champneys or visited him at the University of Bristol. We thank him for discussions and comments as

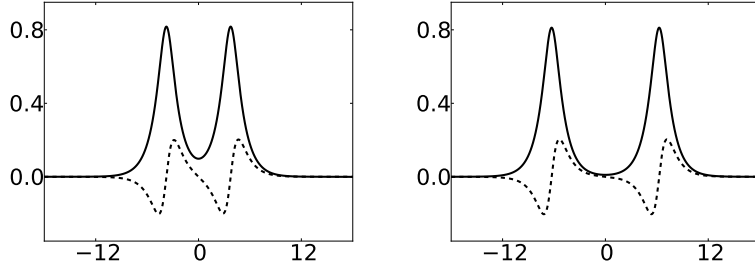


Figure 19: Symmetric, two-pulse GSs with $V = -U^*$ of (2.3) born at the saddle-node bifurcation of Fig. 15(d) for $\varepsilon = 0.01$, $\omega = 0.5$, $\mu = 0$ and $k = 1$.

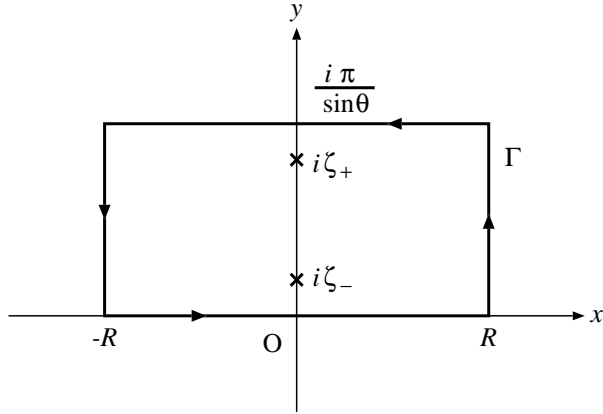


Figure A.1: The rectangle contour Γ .

well as his hospitality and support. K.Y. acknowledges support from the Japan Society for the Promotion of Science, Grant-in-Aid for Scientific Research (C) Nos. 18560056, 21540124 and 22540180.

Appendix A. Derivations of equations (3.6) and (3.7)

Let

$$f_j(x) = \frac{\sinh(2x \sin \theta)}{[\cosh(2x \sin \theta) + \cos \theta]^j}$$

and let

$$I_j = \int_{-\infty}^{\infty} f_j(x) \sin kx \, dx \quad (\text{A.1})$$

for $j = 2, 3$. To estimate (A.1), we consider the complex integral

$$\oint_{\Gamma} f_j(z) e^{ikz} \, dz,$$

where Γ is a rectangle contour, $-R \leq x \leq R$ and $0 \leq y \leq \pi/\sin\theta$, depicted in Fig. A.1, with $R > 0$. The complex function $f_j(z)$ is singular only at

$$z = i\zeta_{\pm}, \quad \zeta_{\pm} = \frac{\pi \pm \theta}{2 \sin \theta},$$

which are j th-order poles, inside of Γ . By the residue theorem, we have

$$\oint_{\Gamma} f_j(z) e^{ikz} dz = 2\pi i \left(\rho_j^{(+)} + \rho_j^{(-)} \right), \quad (\text{A.2})$$

where $\rho_j^{(\pm)}$ is the residue of $f_j(z) \sin kz$ at $z = i\zeta_{\pm}$. We compute

$$\rho_2^{(\pm)} = \mp \frac{ke^{-k\zeta_{\pm}}}{4 \sin^3 \theta}, \quad \rho_3^{(\pm)} = \frac{ke^{-k\zeta_{\pm}}}{16 \sin^5 \theta} (\pm 2 \cos \theta + k),$$

so that

$$\oint_{\Gamma} f_2(z) e^{ikz} dz = i \frac{\pi k}{\sin^3 \theta} \exp\left(-\frac{k\pi}{2 \sin \theta}\right) \sinh\left(\frac{k\theta}{2 \sin \theta}\right)$$

and

$$\begin{aligned} \oint_{\Gamma} f_3(z) e^{ikz} dz &= i \frac{\pi k}{4 \sin^5 \theta} \exp\left(-\frac{k\pi}{2 \sin \theta}\right) \\ &\quad \times \left[-2 \sinh\left(\frac{k\theta}{2 \sin \theta}\right) \cos \theta + k \cosh\left(\frac{k\theta}{2 \sin \theta}\right) \right]. \end{aligned}$$

On the other hand, we can write

$$\begin{aligned} \oint_{\Gamma} f_j(z) e^{ikz} dz &= \int_{-R}^R f_j(x) e^{ikx} dx + i \int_0^{\pi/\sin\theta} f_j(R+iy) e^{ik(R+iy)} dy \\ &\quad + \int_R^{-R} f_j(x+i\pi/\sin\theta) e^{ik(x+i\pi/\sin\theta)} dx \\ &\quad + \int_{\pi/\sin\theta}^0 f_j(-R+iy) e^{ik(-R+iy)} dy. \end{aligned} \quad (\text{A.3})$$

Since by $f_j(x+i\pi/\sin\theta) = f_j(x)$

$$\int_R^{-R} f_j(x+i\pi/\sin\theta) e^{ik(x+i\pi/\sin\theta)} dx = -\exp\left(-\frac{k\pi}{\sin\theta}\right) \int_{-R}^R f_j(x) e^{ikx} dx$$

and the second and fourth integrals in (A.3) tend to zero as $R \rightarrow \infty$, we have

$$\int_{-\infty}^{\infty} f_j(x) e^{ikx} dx = \frac{2\pi i \left(\rho_j^{(-)} + \rho_j^{(+)} \right)}{1 - \exp\left(-\frac{k\pi}{\sin\theta}\right)},$$

where we used (A.2). Hence, we obtain

$$I_2 = \frac{\pi k}{2 \sin^3 \theta} \operatorname{cosech}\left(\frac{k\pi}{2 \sin \theta}\right) \sinh\left(\frac{k\theta}{2 \sin \theta}\right)$$

and

$$I_3 = \frac{\pi k}{8 \sin^5 \theta} \operatorname{cosech}\left(\frac{k\pi}{2 \sin \theta}\right) \left[-2 \sinh\left(\frac{k\theta}{2 \sin \theta}\right) \cos \theta + k \cosh\left(\frac{k\theta}{2 \sin \theta}\right) \right],$$

from which Eqs. (3.6) and (3.7) follow.

Appendix B. Calculation of the boundaries of the central gap via averaging

Applying the third-order averaging method, we calculate the boundaries of the central gap. Again, the *Mathematica* program “haverage.m” is used to obtain the third-order averaged systems.

Appendix B.1. Right boundary

Let $\omega = 1 - \varepsilon^2\nu$ and $\mu = \varepsilon\bar{\mu}$. Using the transformation $(a, b) = (\varepsilon\xi, \varepsilon^{3/2}\eta)$, we rewrite (3.2) as

$$\begin{aligned}\xi' &= -2\varepsilon^{1/2}\eta + \varepsilon^{3/2}[\cos kx - \bar{\mu}\cos(kx + \delta)]\eta + O(\varepsilon^{5/2}), \\ \eta' &= \varepsilon^{1/2}[\cos kx + \bar{\mu}\cos(kx + \delta)]\xi + \varepsilon^{3/2}\left(-\nu\xi + \frac{3}{2}\xi^3\right) + O(\varepsilon^{5/2}).\end{aligned}\tag{B.1}$$

The third-order averaged system for (B.1) is obtained as

$$\xi' = -2\varepsilon^{1/2}\eta, \quad \eta' = \varepsilon^{3/2}\left[-\left(\nu - \frac{6}{k^2}(1 + \bar{\mu}^2 + 2\bar{\mu}\cos\delta)\right)\xi + \frac{3}{2}\xi^3\right],\tag{B.2}$$

where $\varepsilon^{1/2}$ was taken as the small parameter. In the averaged system (B.2), the origin is a saddle if

$$\nu > \frac{6}{k^2}(1 + \bar{\mu}^2 + 2\bar{\mu}\cos\delta).$$

Hence, we have the approximate right boundary of the central gap,

$$\omega = 1 - \frac{6\varepsilon^2}{k^2}(1 + \bar{\mu}^2 + 2\bar{\mu}\cos\delta).$$

Appendix B.2. Left boundary

Let $\omega = -1 + \varepsilon^2\nu$ and $\mu = \varepsilon\bar{\mu}$. Using the transformation $(a, b) = (\varepsilon^{3/2}\xi, \varepsilon\eta)$, we rewrite (3.2) as

$$\begin{aligned}\xi' &= \varepsilon^{1/2}[\cos kx - \bar{\mu}\cos(kx + \delta)]\eta - \varepsilon^{3/2}\left(\nu\eta + \frac{3}{2}\eta^3\right) + O(\varepsilon^{5/2}), \\ \eta' &= -2\varepsilon^{1/2}\xi + \varepsilon^{3/2}[\cos kx + \bar{\mu}\cos(kx + \delta)]\xi + O(\varepsilon^{5/2}),\end{aligned}\tag{B.3}$$

The third-order averaged system for (B.3) is obtained as

$$\xi' = \varepsilon^{3/2}\left[-\left(\nu - \frac{6}{k^2}(1 + \bar{\mu}^2 - 2\bar{\mu}\cos\delta)\right)\eta - \frac{3}{2}\eta^3\right], \quad \eta' = -2\varepsilon^{1/2}\xi,$$

in which the origin is a saddle if

$$\nu > \frac{6}{k^2}(1 + \bar{\mu}^2 - 2\bar{\mu}\cos\delta).\tag{B.4}$$

Thus, we have the approximate left boundary of the central gap,

$$\omega = 1 - \frac{6\varepsilon^2}{k^2}(1 + \bar{\mu}^2 - 2\bar{\mu}\cos\delta).$$

References

- [1] A. B. Aceves and S. Wabnitz, Self-induced transparency solitons in nonlinear refractive periodic media, *Phys. Lett. A* 141 (1989) 37–42.
- [2] B. B. Baizakov, V. V. Konotop, and M. Salerno, Regular spatial structures in arrays of Bose-Einstein condensates induced by modulational instability, *J. Phys. B: At. Mol. Opt. Phys.* 35 (2002) 5105–5119.
- [3] I. V. Barashenkov, D. E. Pelinovsky, and E. V. Zemlyanaya, Vibrations and oscillatory instabilities of gap solitons, *Phys. Rev. Lett.* 80 (1998) 5117–5120.
- [4] V. A. Brazhnyi and V. V. Konotop, Theory of nonlinear matter waves in optical lattices, *Mod. Phys. Lett. B* 18(2004) 627–651.
- [5] N. G. R. Broderick and C. M. de Sterke, Theory of grating superstructures, *Phys. Rev. E* 55 (1997) 3634–3646.
- [6] B. Buffoni, A. R. Champneys and J. F. Toland, Bifurcation and coalescence of a plethora of homoclinic orbits for a Hamiltonian system, *J. Dynam. Differential Equations* 8 (1996) 221–279.
- [7] D. N. Christodoulides and R. I. Joseph, Slow Bragg solitons in nonlinear periodic structures, *Phys. Rev. Lett.* 62 (1989) 1746–1749.
- [8] M. Chugunova and D. Pelinovsky, Block-diagonalization of the symmetric first-order coupled-mode system, *SIAM J. Appl. Dyn. Syst.* 5 (2006), 66–83.
- [9] G. Derks and G. A. Gottwald, A robust numerical method to study oscillatory instability of gap solitary waves, *SIAM J. Appl. Dyn. Syst.* 4 (2005), 140–158.
- [10] C. M. de Sterke and J. E. Sipe, Gap solitons, *Progr. Opt.* 33 (1994) 203–260.
- [11] E. J. Doedel, A. R. Champneys, T. R. Fairgrieve, Yu. A. Kuznetsov, B. Sandstede, and X. J. Wang, AUTO97 Continuation and Bifurcation Software for Ordinary Differential Equations, 1997 (an upgraded version is available at <http://cmv1.cs.concordia.ca/auto/>).
- [12] T. Dohnal, D. E. Pelinovsky and G. Schneider, Coupled-mode equations and gap solitons in a two-dimensional nonlinear elliptic problem with a separable periodic potential, *J. Nonlinear Sci.* 19 (2009) 95–131.
- [13] T. Dohnal and H. Uecker, Coupled mode equations and gap solitons for the 2D Gross-Pitaevskii equation with a non-separable periodic potential, *Phys. D* 238 (2009) 860–879.
- [14] B. J. Eggleton, C. M. de Sterke, and R. E. Slusher, Bragg solitons in the nonlinear schrodinger limit: experiment and theory, *J. Opt. Soc. Am. B* 16 (1999) 587–599.
- [15] B. J. Eggleton, R. E. Slusher, C. M. de Sterke, P. A. Krug, and J. E. Sipe, Bragg grating solitons, *Phys. Rev. Lett.* 76 (1996) 1627–1630.
- [16] B. Eiermann, T. Anker, M. Albiez, M. Taglieber, P. Treutlein, K.-P. Marzlin, and M. K. Oberthaler, Bright bose-einstein gap solitons of atoms with repulsive interaction, *Phys. Rev. Lett.*, 92, 2004.
- [17] J. Guckenheimer and P. Holmes, *Nonlinear Oscillations, Dynamical Systems and Bifurcations of Vector Fields*, Springer, New York, 1983.
- [18] G. Hwanga, T. R. Akylas and J. Yang Gap solitons and their linear stability in one-dimensional periodic media, *Phys. D* 240 (2011) 1055–1068.
- [19] B. Ilan and M. I. Weinstein, Band-edge solitons, nonlinear Schrödinger/Gross-Pitaevskii equations, and effective media, *Multiscale Model. Simul.* 8 (2010) 1055–1101.
- [20] T. Kapitula, Stability of waves in perturbed Hamiltonian systems, *Phys. D* 156 (2001)186–200.
- [21] R. Kashyap, *Fiber Bragg gratings*, Academic Press, San Diego, 1999.
- [22] J. Knobloch, Bifurcation of degenerate homoclinics in reversible and conservative systems, *J. Dynam. Differential Equations*, 9 (3): 427–444, 1997.
- [23] J. S. W. Lamb and J. A. G Roberts, Time-reversal symmetry in dynamical systems: A survey, *Phys. D* 112 (1998) 1–39.

- [24] P. J. Y. Louis, E. A. Ostrovskaya, and Y. S. Kivshar, Dispersion control for matter waves and gap solitons in optical superlattices, *Phys. Rev. A* 71 (2005) 023612.
- [25] W. C. K. Mak, B. A. Malomed, and P. L. Chu, Slowdown and splitting of gap solitons in apodized Bragg gratings, *J. Mod. Opt.* 51 (2004) 2141–2158.
- [26] B. A. Malomed and R. S. Tasgal, Vibration modes of a gap soliton in a nonlinear optical medium, *Phys. Rev. E*, 49 (1994) 5787–5796.
- [27] J. T. Mok, C. M. de Sterke, I. C. M. Litter, and B. J. Eggleton, Dispersionless slow light using gap solitons, *Nature Phys.* 2 (2006) 775–780.
- [28] J. Murdock. *Qualitative theory of nonlinear resonance by averaging and dynamical systems methods*, in: U. Kirchgraber and H.-O. Walther (Eds.), *Dynamics Reported*, Vol. 1, Wiley, New York, 1988, pp. 91–172.
- [29] J. Murdock, *Perturbations: Theory and Methods*, Wiley, New York, 1991.
- [30] A. I. Neishtadt, The separation of motions in systems with rapidly rotating phase, *J. Appl. Math. Mech. (PMM)* 48 (1984) 133–139.
- [31] E. A. Ostrovskaya and Y. S. Kivshar, Matter-wave gap solitons in atomic band-gap structures, *Phys. Rev. Lett.* 90 (2003) 160407.
- [32] D. E. Pelinovsky and G. Schneider, Justification of the coupled-mode approximation for a nonlinear elliptic problem with a periodic potential, *Appl. Anal.* 86 (2007) 1017–1036.
- [33] D. E. Pelinovsky, A. A. Sukhorukov and Y. S. Kivshar, Bifurcations and stability of gap solitons in periodic potentials, *Phys. Rev. E* 70 (2004) 036618.
- [34] M. A. Porter and P. G. Kevrekidis, Bose-Einstein condensates in superlattices, *SIAM J. Appl. Dyn. Syst.* 4 (2005) 783–807.
- [35] P. St. J. Russell, Optical superlattices for modulation and deflection of light, *J. Appl. Phys.* 59 (1986) 3344–3355.
- [36] R. E. Slusher, B. J. Eggleton, T. A. Strasser and M. de Sterke, Nonlinear pulse reflections from chirped fiber gratings, *Opt. Expr.* 3 (1998) 465–475.
- [37] P. Smith and D. W. Jordan, *Nonlinear Ordinary Differential Equations: An Introduction to Dynamical Systems*, Oxford University Press, Oxford, 3rd ed., 1999.
- [38] L. N. Trefethen, *Spectral Methods in MATLAB*, SIAM, Philadelphia, 2000.
- [39] G. Van Simaey, S. Coen, M. Haelterman, and S. Trillo, Observation of resonance soliton trapping due to a photoinduced gap in wave number, *Phys. Rev. Lett.* 92 (2004) 223902.
- [40] C. Simó, Averaging under fast quasiperiodic forcing, in: J. Seimenis (Ed.), *Hamiltonian mechanics: Integrability and chaotic behavior, Proceedings of a NATO Advanced Research Workshop held in Toruń, June 28-July 2, 1993*, Plenum, New York, 1994, pp. 13–34.
- [41] S. Wiggins, *Introduction to Applied Nonlinear Dynamical Systems and Chaos*, Springer, New York, 1990.
- [42] S. Wolfram, *The Mathematica Book*, 5th ed. Wolfram Media, Champaign, IL, 2003.
- [43] K. Yagasaki. Numerical detection and continuation of homoclinic points and their bifurcations for maps and periodically forced systems. *Int. J. Bifurcation Chaos* 8 (1998) 1617–1627.
- [44] K. Yagasaki, HomMap: An Auto driver for homoclinic bifurcation analysis of maps and periodically forced systems, 1998, available from http://www.eng.niigata-u.ac.jp/~yagasaki/software_e.html.
- [45] K. Yagasaki, Higher-order averaging and ultra-subharmonics in forced oscillators, *J. Sound Vib.* 210 (1998) 529–553.
- [46] K. Yagasaki. Detection of bifurcation structures by higher-order averaging for Duffing’s equation. *Nonlinear Dynamics* 18 (1999) 129–158.
- [47] K. Yagasaki, Nonlinear dynamics and bifurcations in external feedback control of microcantilevers in atomic force microscopy, Submitted for publication.

- [48] K. Yagasaki and T. Ichikawa, Higher-order averaging for periodically forced weakly nonlinear systems, *Int. J. Bifurcation Chaos* 9 (1999) 519–531.
- [49] K. Yagasaki, I. M. Merhasin, B. A. Malomed, T. Wagenknecht and A. R. Champneys, Gap solitons in Bragg gratings with a harmonic superlattice, *Europhys. Lett.* 74 (2006) 1006–1012.